NTNU

Norwegian University of
Science and Technology

Production Data Analysis During Transient Linear Flow in Shale Gas Reservoirs

Magnus Edvard Nystad

Petroleum Geoscience and Engineering
Submission date: January 2017
Supervisor: Curtis Hays Whitson, IGP

Norwegian University of Science and Technology
Department of Geoscience and Petroleum

Abstract

This work investigates the application of a graphical straight-line method often used to calculate the product of fracture half-length and the square root of permeability for hydraulically fractured shale gas wells. The analysis is based on the transient linear flow regime, as this flow regime is documented to be dominant in many fractured unconventional formations (Wattenbarger et al. 1998, Bello 2009). The equation used to generate the diagnostic plot utilized in the analysis is derived from basic fluid flow principles, where an equation relying on constant flow rate is modified to accommodate varying rate production data by use of superposition.

To accurately describe gas flow in shale reservoirs, the model needs to consider that several of the parameters used in the analysis are pressure sensitive, such as gas viscosity, reservoir porosity, gas compressibility and the amount free gas introduced to the flow system by the process of desorption. These pressure dependent properties will all influence the solution to the governing equation, where changes in the diffusivity term, $k/(\phi\mu c_t)$, are implemented in the analysis by use of pseudofunctions and correction factors. Three methods to account for pressure sensitive parameters in the diffusivity term are investigated in this work, where two of the methods are modified by the author to be applicable to varying flowing pressure conditions. It was found that all three methods improve the analysis when applied to simulated data, but better results were obtained from the modified Behmanesh (2016) method and the methodology proposed by Nobakht and Clarkson (2011a, 2011b, 2011c) and Nobakht et al. (2011).

Sammendrag

Dette arbeidet undersøker anvendelsen av en grafisk rett-linje metode ofte brukt til å beregne produktet av halv sprekklengde og kvadratroten til permabilitet i hydraulisk frakturerte skifergassbrønner. Analysen er basert på det transiente lineære strømningsregimet, da dette strømningsregimet ofte forekommer i frakturerte ukonvensjonelle formasjoner (Wattenbarger et al. 1998, Bello 2009). Ligningen brukt til å generere det diagnostiske plottet anvendt i denne studien er utledet fra generelle prinsipper, hvor en ligning basert på konstant strømningsrate er gjort i stand til å brukes for varierende strømningsrate ved hjelp av superposisjon.

For å beskrive gasstrømmen i skifergassreservoarer, må den brukte modellen ta hensyn til at flere av parameterne som brukes i analysen er trykkfølsome, slik som gassviskositet, reservoarporøsitet, gasskompressibilitet og mengden fri gass introdusert til strømningssystemet gjennom desorpsjon. Disse trykkavhengige egenskapene vil påvirke ligningen brukt til å beskrive systemet, hvor forandringer i diffusivitetsleddet, $k/(\phi\mu c_t)$, er implementert i analysen ved hjelp av pseudofunksjoner og korreksjonsfaktorer. Tre metoder brukt til å ta hensyn til trykksensitive parametere i diffusivitetsleddet er undersøkt i denne studien, hvorav to av metodene er modifisert av forfatteren til å kunne brukes for varierende bunnhullstrykk. Undersøkelsen viser at alle tre metodene forbedrer analyseresultatene når de anvendes på simulert data, der de beste resultatene ble oppnådd fra den modifiserte Behmanesh (2016) metoden og fra metodikken foreslått av Nobakht og Clarkson (2011a, 2011b, 2011c) og Nobakht et al. (2011).

Acknowledgements

I would like to thank my thesis supervisor, professor Curtis Hays Whitson, for his guidance and help during my final years at NTNU. I would also like to express my sincerest gratitude to my parents, for their continuous support and affection. Finally, I would like to thank all the wonderful people I have met during my time as a student, that has made my time at NTNU the best years of my life.

Table of Contents

List of Figures

List of Tables

1 Production Data Analysis in Shale Gas Reservoirs

With an ever-rising demand for energy, the development of unconventional reservoirs such as gas shales are becoming increasingly relevant. Because of their low permeability, these reservoirs must be stimulated to produce at economic flow rates. This is often done with horizontal wells with multiple hydraulic fracture stages. This technique exposes the formation to large fracture areas that can be considered extensions of the wellbore, acting as fluid flow conduits transporting the reservoir fluids from the low permeability reservoir and into the wellbore.

The flow geometry created in these hydraulically fractured wells has received a great deal of attention in the literature. Clarkson and Pedersen (2010) has provided an overview of possible conceptual reservoir/fracture geometries used to analyze production data in fractured tight reservoirs, ranging from parallel planar fractures perpendicular to the horizontal well to complex fracture networks. The dominant flow regime in many of these wells is reported in the literature to be transient linear flow in both the planar fracture model (Wattenbarger, 1998) and in the fracture network models (Bello, 2009). A technique to identify the source of the transient linear flow as either dominated by matrix flow to the fractures or flow in the fracture system by analyzing production data from two nearby wells has been proposed by Kanfar et al. (2013).

The successful modeling of fluid flow is integral for estimating reserves and optimizing drilling and completion strategies, to make production from low permeability formations such as shale gas reservoirs economically viable. Clarkson (2013) divide the analysis of production data from unconventional gas wells into five different categories:

1. *Straight-line (or flow regime) methods* that utilize specialty plots designed to linearize the dataset for a given flow regime. Depending on the flow geometry, different reservoir and/or completion properties may be obtained.
2. *Type curve methods* that involve matching of production data to dimensionless flow equation solutions. These type curves typically capture multiple flow regimes, and unique matches can yield reservoir or completion parameters.
3. *Analytical and numerical simulation methods,* which are based on creating a representative model of the reservoir and using this model to generate type curves for type curve matching, solving for reservoir and completion parameters through history

matching, and to generate production forecasts. Analytical models are in general employed for relatively simple reservoir behavior and are based on solutions to analytically derived mathematical models. Numerical simulation models have the potential to solve more complex mathematical scenarios using numerical methods such as finite difference and finite element.

4. *Empirical methods* employ empirically obtained fluid flow equations, which are calibrated to match the observed production data and can be extrapolated to predict future production.
5. *Hybrid methods* combine analytical solutions to model and forecast transient and transitional flow and empirical relations to model and forecast the boundary dominated flow period.

To gain as much knowledge as possible about the reservoir, a combination of these analysis methods should be employed, as they can complement each other or confirm what was indicated by a different analysis. This presupposes that the fundamental reservoir description is adhered to in all the analysis methods applied (Whitson et al. 2016).

The focus of this work is on a straight-line method from the first category. Because of the prevalence of transient linear flow in fractured shale gas reservoirs, the analysis method is based on this flow regime. Several ways of correcting for pressure dependent parameters are investigated to improve the accuracy of the straight-line analysis.

This study is a continuation of the investigation performed by Nystad (2015). For completeness, modified versions of several of the sections found in Nystad (2015) are included in this work.

2 Rate Transient Analysis – A Straight-Line Method

Rate transient analysis is a form of production data analysis that accounts for the changing operating conditions of the well by including both varying rates and varying flowing pressures. By use of mathematical formulations such as superposition (convolution), the production data can be made to follow constant rate or constant flowing pressure behavior, which again can be used to analyze data on specialized diagnostic plots. These plots are specialized in the sense that they assume that a specific flow regime is dominant, and that analytical equations based on that flow regime will linearize the data so that information can be extracted.

2.1 The Reservoir Model

The reservoir/fracture geometry investigated in this work is depicted in **Fig. 2.1**, which shows a rectangular reservoir with a hydraulic fracture extending from the centered wellbore to the outer reservoir boundaries. This model is conceptually applicable to either a vertical well with a single hydraulic fracture, or a section of a horizontal well with multiple hydraulic fractures, as shown in **Fig. 2.2**. The reservoir area drained by the fracture is assumed to be equal to the fracture length multiplied by the reservoir width, $A = 2x_f \cdot 2y_e = 2x_e \cdot 2y_e$, so that production from the region beyond the tip of the fracture is neglected. The fracture is assumed to have infinite conductivity and to penetrate the entire height of the formation. With these assumptions, the flow regime will be transient linear flow until the no-flow boundary is reached and boundary dominated flow sets in. Infinite fracture conductivity is a good assumption when the dimensionless fracture conductivity, F_{CD}, is larger than 50 (Ibrahim and Wattenbarger, 1998). The dimensionless fracture conductivity is defined as

$$F_{CD} = \frac{k_f w_f}{k x_f}, \quad \text{.....(2.1)}$$

where k_f and k are fracture and formation permeabilities, respectively, w_f is the fracture width and x_f is the fracture half length, all in consistent units.

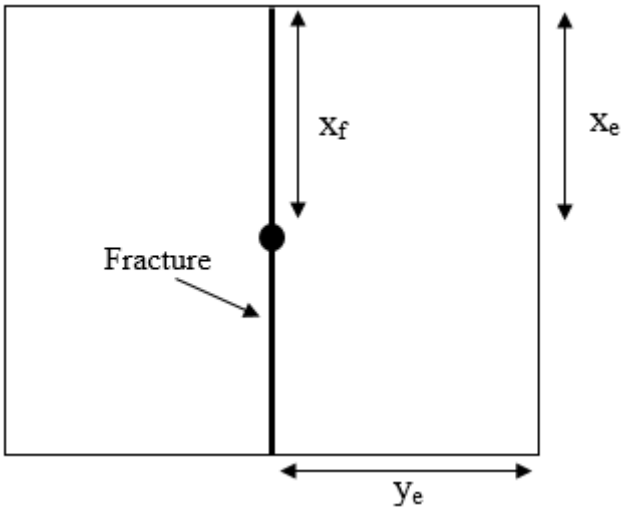

Fig. 2.1 - Rectangular reservoir with a single hydraulic fracture extending to the reservoir boundaries.

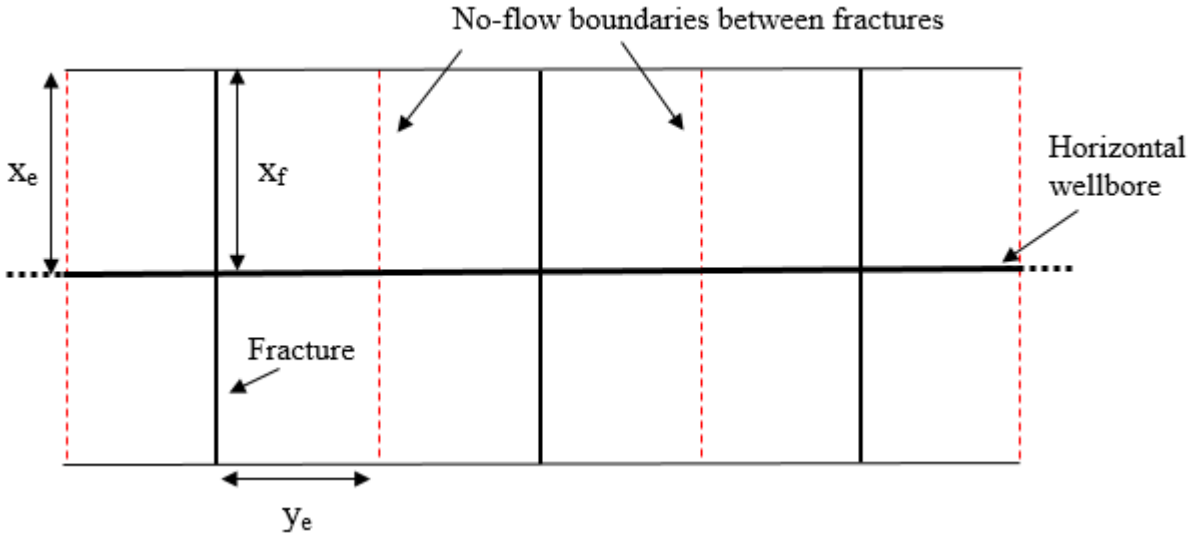

Fig. 2.2 - Horizontal well with equally spaced hydraulic fractures.

Fig. 2.2 shows a segment of a horizontal well with *n* equally spaced hydraulic fractures. It is assumed that the reservoir is homogeneous and that all fracture properties (such as half-length and conductivity) are equal. The individual fractures are producing into a common wellbore, and thus at the same pressure. Under these assumptions, each fracture will have the same drainage area, with no-flow boundaries halfway between adjacent fractures. The fractured horizontal well will therefore behave like *n* independent single fracture wells, and can be modelled by the geometry shown in Fig. 2.1, with the results scaled to account for the number of fractures. Because of this property, all simulations performed in this work are done with the single fracture model.

2.2 A Straight-Line Method

The modeling of fluid flow in porous media is based on the diffusivity equation, which is obtained by combining the law of conservation of mass, Darcy's law, and an appropriate equation of state for the fluid system. In the case of one dimensional flow, the diffusivity equation can be formulated in dimensionless variables as

$$\frac{\partial^2 p_D}{\partial y_D^2} = \frac{\partial p_D}{\partial t_D}, \quad \text{.....(2.2)}$$

where p_D is dimensionless pressure, y_D is dimensionless distance and t_D is dimensionless time. The definitions of these dimensionless variables vary per the reservoir geometry and fluid system. For a low-pressure gas (p_i < 2000 psia), the dimensionless pressure is defined as

$$p_D = \frac{0.703kh}{q_g \mu_g ZT}\left(p_i^2 - p_{wf}^2\right). \quad \text{.....(2.3)}$$

Here, k is permeability in md, h is reservoir height in ft, q_g is gas rate in scf/D, μ_g is gas viscosity, Z is the dimensionless gas deviation factor, T is reservoir temperature in °R, and p_i and p_{wf} are initial and wellbore flowing pressure, respectively, given in psia. The use of Eq. 2.3 assumes that the product of the deviation factor and gas viscosity is approximately constant, which is a valid assumption only for relatively low pressures. This limitation can be circumvented by using real gas pseudopressure (Al-Hussainy et al. 1966),

$$p_p(p) = \int_{p_0}^{p} \frac{p}{\mu(p)Z(p)} dp, \quad \text{.....(2.4)}$$

given in psia^2/cP, where p_0 is some arbitrarily chosen low pressure such as 14.7 psia. Using Eq. 2.4, the dimensionless pressure can be expressed as

$$p_D = \frac{0.703kh}{q_g T}\left(p_p(p_i) - p_p(p_{wf})\right). \quad \text{.....(2.5)}$$

It can be seen by substituting Eq. 2.4 into Eq. 2.5 and assuming that the viscosity-gas deviation factor product is constant that the two dimensionless pressure definitions are equivalent. Eq. 2.5 is the dimensionless pressure equation used in this work, as it accounts for the changes in viscosity and gas deviation factor, and can be applied to a wide range of reservoir pressures.

The dimensionless time used in Eq. 2.2 is defined for a hydraulically fractured reservoir with a fracture half-length of x_f feet as

$$t_{Dxf} = \frac{0.00633k}{(\phi\mu c_t)_i x_f^2} t = t_{Dxfc} t. \quad \text{.....(2.6)}$$

Here, t is time in days, ϕ is porosity as a fraction, c_t is total system compressibility in psi^{-1}, defined for a fully saturated gas reservoir as the summation of gas compressibility and formation compressibility. The subscript i symbolizes that the parameters are evaluated at the initial conditions. A dimensionless time constant is also defined so that $t = t_{Dxf}/t_{Dxfc}$. The dimensionless time constant is strictly speaking not a constant, since it contains several parameters that are functions of pressure, when the fluid is a gas. This will be discussed further in chapter 2.4.

Given a set of initial and boundary conditions, solutions to Eq. 2.2 are given on the form $p_D = f(y_D, t_D)$, which is reduced to $p_D = f(t_D)$ when evaluated at the face of the fracture, where the dimensionless distance, $y_D = y/x_f$, is equal to zero. When skin in present, the dimensionless pressure equation is expressed as $p_{D,real} = p_{D,ideal} + s$, where s is a dimensionless skin factor. To distinguish between which boundary condition is used to solve Eq. 2.2, the notation p_D is used for constant rate production, while $1/q_D$ is used for constant pressure production. When the constant flowing pressure boundary condition is used to solve Eq. 2.2, the reciprocal of dimensionless rate is substituted for dimensionless pressure in the previously defined equations. This distinction is important, because the constant rate and constant pressure solutions are not identical for the transient linear flow regime.

Since the dimensionless pressure can be expressed as a function of dimensionless time, Eq. 2.5 can be formulated as

$$p_D(t_D) = \frac{0.703kh}{T} \frac{\left(p_p(p_i) - p_p(p_{wf})\right)}{q_g} = p_{Dc} \frac{\left(p_p(p_i) - p_p(p_{wf})\right)}{q_g}, \quad \text{.....(2.7)}$$

which gives a pressure-time relationship for a well producing at a constant rate. A dimensionless pressure constant is also defined so that $\Delta p_p/q_g = p_D/p_{Dc}$. Wells don't usually produce at a constant rate, therefore Eq. 2.7 needs to be modified to be valid for varying production rates. This is done with the principle of superposition, which is a mathematical formulation that accounts for variations in rate (or pressures, if applied to the constant pressure solution). A rate change of Δq at time t is incorporated into the analysis by

adding a new "imaginary well" on top of the original well, with the new well starting production at time t and producing at a constant rate equal to Δq, while the original well keeps producing at the initial rate. This procedure can be repeated for a sequence of rate changes.

As shown by Fetkovich and Vienot (1984), a generalized version of Eq. 2.7 that accounts for varying production rates with superposition can be expressed as

$$p_p(p_i) - p_p(p_{wf}) = \frac{1}{p_{Dc}}\left[\sum_{j=1}^{n}\left(q_j - q_{j-1}\right)\left[p_D\left(t_{Dn} - t_{Dj-1}\right) + s\right]\right]. \quad \text{.....(2.8)}$$

Since the sum of the rate changes in Eq. 2.8, $\sum_{j=1}^{n}(q_j - q_{j-1})$, is equal to the rate at timestep *n*, q_n, the summation term on the right-hand side of the equation can be expressed as

$$\sum_{j=1}^{n}\left(q_j - q_{j-1}\right)\left[p_D\left(t_{Dn} - t_{Dj-1}\right) + s\right] = q_n s + \sum_{j=1}^{n}\left(q_j - q_{j-1}\right)p_D\left(t_{Dn} - t_{Dj-1}\right). \quad \text{.....(2.9)}$$

To avoid the unknown skin factor being multiplied by a changing rate, Odeh and Jones (1965) suggest normalizing the equation by dividing both sides of Eq. 2.8 by q_n;

$$\frac{p_p(p_i) - p_p(p_{wf})}{q_n} = \frac{1}{p_{Dc}}\left[s + \sum_{j=1}^{n}\frac{\left(q_j - q_{j-1}\right)}{q_n}p_D\left(t_{Dn} - t_{Dj-1}\right)\right]. \quad \text{.....(2.10)}$$

This generalized equation can be applied to any flow regime, if the correct dimensionless pressure function is used. For the transient linear flow regime, the dimensionless pressure solution for constant rate production is (Gringarten et al. 1974)

$$p_D\left(t_{Dxf}\right) = \sqrt{\pi t_{Dxf}} = \sqrt{\pi t_{Dxfc}}\sqrt{t}. \quad \text{.....(2.11)}$$

Substituting Eq. 2.11 into Eq. 2.10 yields

$$\frac{p_p(p_i) - p_p(p_{wf})}{q_n} = \frac{1}{p_{Dc}}\left[s + \sqrt{\pi t_{Dxfc}}\sum_{j=1}^{n}\frac{\left(q_j - q_{j-1}\right)}{q_n}\sqrt{t_n - t_{j-1}}\right]. \quad \text{.....(2.12)}$$

Using the notation t_{LS} for linear superposition time, defined by Clarkson and Beierle (2010) as

$$t_{LS} = \sum_{j=1}^{n}\frac{\left(q_j - q_{j-1}\right)}{q_n}\sqrt{t_n - t_{j-1}}, \quad \text{.....(2.13)}$$

allows Eq. 2.12 to be formulated in a more convenient way;

$$\frac{p_p(p_i)-p_p(p_{wf})}{q_n}=\frac{s}{p_{Dc}}+\frac{\sqrt{\pi t_{Dxfc}}}{p_{Dc}}t_{LS}. \quad \text{.....(2.14)}$$

It can be noted that for constant rate conditions, the linear superposition time is equal to the square root of time. As seen from Eq. 2.14, a Cartesian plot of normalized pseudopressure drawdown versus linear superposition time will form a straight line with a slope, m_{CR}, of

$$m_{CR}=\frac{\sqrt{\pi t_{Dxfc}}}{p_{Dc}}=\frac{0.2006T}{h\sqrt{(\phi\mu c_t)_i}}\frac{1}{x_f\sqrt{k}} \quad \text{.....(2.15)}$$

if the flow regime is transient linear. This plot will henceforth be referred to as a Linear Flow Diagnostic Plot (LFDP). The subscript *CR* refers to the constant rate solution used to derive the equation. Eq. 2.15 is normally used to solve for the Linear Flow Parameter (LFP), the product of fracture half-length and the square root of permeability, by rearranging it to

$$x_f\sqrt{k}=\frac{0.2006T}{h\sqrt{(\phi\mu c_t)_i}}\frac{1}{m_{CR}}. \quad \text{.....(2.16)}$$

The intercept on the LFDP will be given by

$$b=\frac{s}{p_{Dc}}=\frac{T}{0.703kh}s, \quad \text{.....(2.17)}$$

which can be used to solve for either permeability or skin if the other parameter is known.

Eqs. 2.8 through 2.17 were derived from the constant rate solution to Eq. 2.2, and are valid for varying rate conditions through the use of superposition. This means that they can also be applied to constant pressure data, which is just a special case of varying rate where the flowing pressure is held constant. Because of this property, the analysis method investigated in this work is based on Eq. 2.14. For completeness, the constant pressure solution to Eq. 2.2 is also included (Wattenbarger et al. 1998);

$$\frac{1}{q_D}=\frac{\pi}{2}\sqrt{\pi t_{Dxf}}=\frac{\pi}{2}\sqrt{\pi t_{Dxfc}}\sqrt{t}, \quad \text{.....(2.18)}$$

which differs from the constant rate solution by a factor of π/2. Combining and rearranging Eq. 2.18 and Eq. 2.7 yields

$$\frac{p_p(p_i)-p_p(p_{wf})}{q_n}=\frac{s}{p_{Dc}}+\frac{\pi}{2}\frac{\sqrt{\pi t_{Dxfc}}}{p_{Dc}}\sqrt{t}. \quad \text{.....(2.19)}$$

The slope of a plot of normalized pseudopressure drawdown versus the square root of time, in this work referred to as a square root of time plot, can therefore be used to solve for the linear flow parameter using the relation

$$x_f \sqrt{k} = \frac{\pi}{2} \frac{0.2006T}{h\sqrt{(\phi\mu c_t)_i}} \frac{1}{m_{CP}}, \quad \text{.....(2.20)}$$

where the subscript *CP* signifies that the constant pressure solution was used to obtain the slope. The intercept of the square root of time plot is described by Eq. 2.17.

2.3 Distance of Investigation

The Distance of Investigation (DOI) concept is analogous to the more commonly used radius of investigation, but is better suited to describe the reservoir geometry shown in Fig. 2.1. The DOI refers to how far a pressure wave, originated at the wellbore, has diffused through the reservoir at a given time, as described by Eq. 2.2. For the DOI concept to be used quantitatively, the pressure disturbance needs to be of a magnitude that exceeds the pressure gauge resolution used to measure it (Kuchuk 2009), and modified per the resolution of the analysis method used (e.g. observable deviations in the production data trends as a reservoir boundary is encountered by the DOI) Daungkaew et al. (2000).

The DOI definition used in this work stems from the work of Muskat (1937), who showed that at an instant of time, transient flow can be approximated as Pseudo Steady State (PSS) flow with boundary conditions dictated by the pressure distribution at that instant. This concept can be utilized by modeling an infinite acting reservoir as having boundaries with positions defined by the expanding DOI, so that at any given time the reservoir is approximated as a closed reservoir in PSS. Authors such as Shahamat et al. (2014) and Behmanesh (2016) have successfully used series of successive pseudo steady states to model transient linear flow in unconventional reservoirs. This concept can also be used to define the investigated reservoir volume at a given time to calculate average gas properties within that region.

The generally used definition of the DOI equation is given as (Kuchuk 2009, Behmanesh et al. 2014, 2015)

$$y_{inv} = \alpha \sqrt{\frac{kt}{(\phi\mu c_t)_i}}, \quad \text{.....(2.21)}$$

where y_{inv} is the investigated distance in feet, measured from the fracture face, and α is a numerical constant that varies with boundary conditions, flow regime and which method was used to derive the constant. Several values for α have been suggested in the literature for transient linear flow, and are summarized in **Table 1**. In this work, the DOI constants used by Nobakht and Clarkson (2011a, 2011b) and the constant pressure DOI constant, α = 0.194, derived by Behmanesh et al. (2014, 2015) are used to estimate a region of investigation, which is assumed to be representable of the reservoir volume from which the fluids are being produced.

The boundary of the investigated region per the different DOI constants in Table 1 are shown together with the pressure profile in the reservoir after two years of production in **Fig. 2.3** for constant flowing pressure production and in **Fig. 2.4** for constant rate production. The data is taken from simulation cases no. 2 and 32, presented in chapter 3.

Table 1 - Different values for the distance of investigation constant.

Derivation method	**Source**	α_{CP}	α_{CR}
Type-curve deviation	Wattenbarger et al. (1998)	0.159	0.113
Type-curve deviation	Arevalo-Villegran et al (2003)	0.1779	0.1591
Empirical	Nobakht & Clarkson (2011a, 2011b)	0.203	0.113
Analytical, unit impulse	Behmanesh et al. (2014,2015)	0.194	0.113
Type-curve intersection	Behmanesh et al. (2014,2015)	0.180	0.141

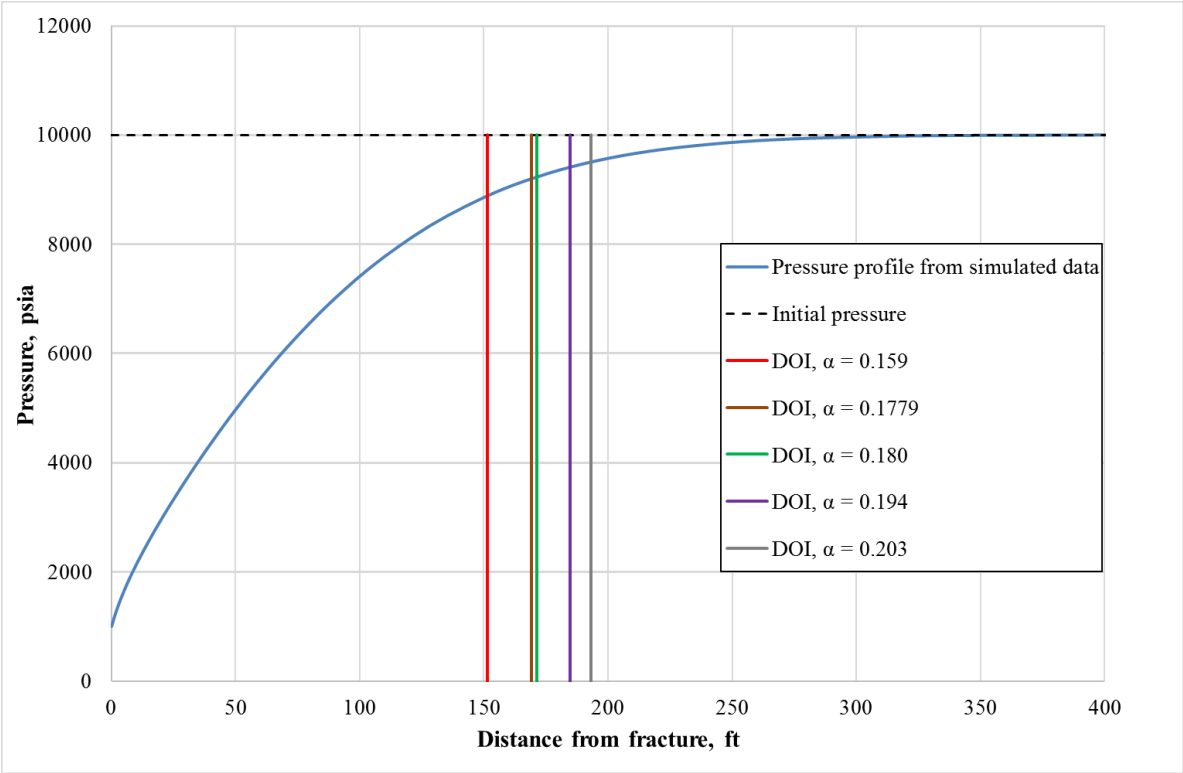

Fig. 2.3 - Pressure profile in the reservoir and estimated DOI after two years of constant pressure production. Data taken from simulation case no. 2.

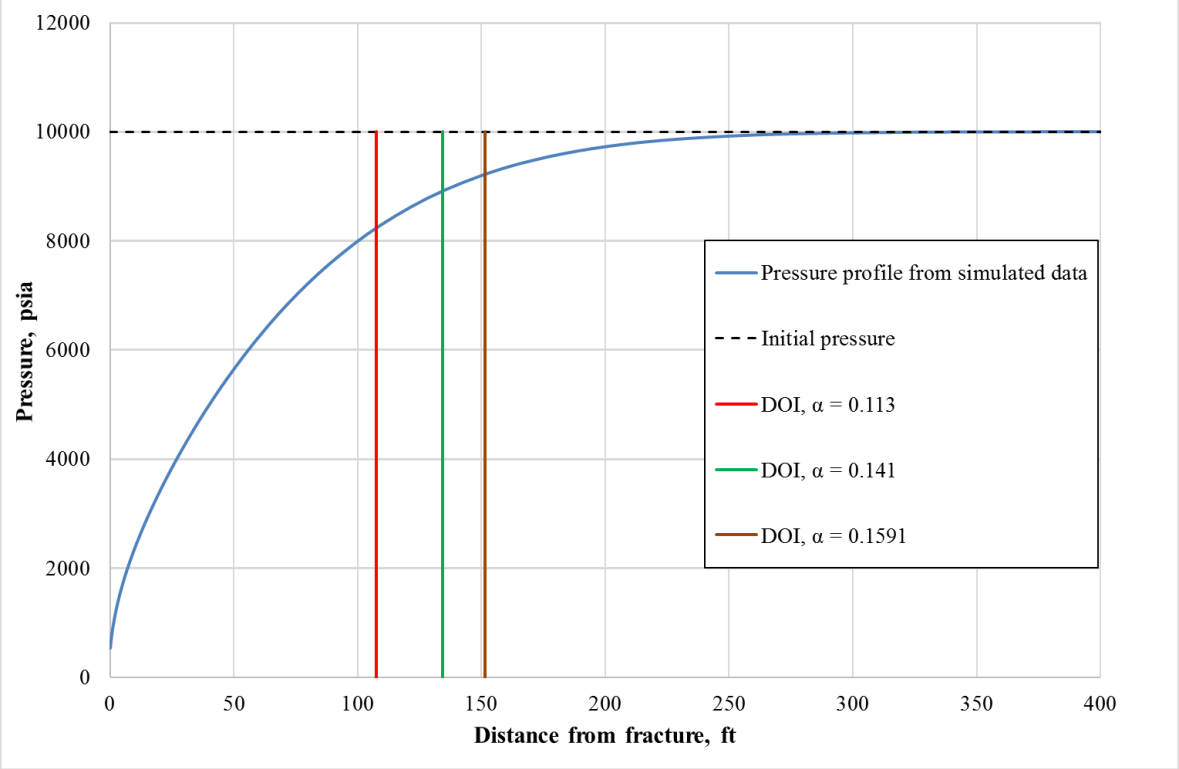

Fig. 2.4 - Pressure profile in the reservoir and estimated DOI after two years of constant rate production. Data taken from simulation case no. 32.

2.4 Accounting for Pressure Dependent Parameters in the Dimensionless Time

The dimensionless time constant defined in Eq. 2.6 is in fact not a constant when the reservoir fluid is a gas, as it contains several parameters that are functions of pressure. Because shale gas reservoirs are often produced at a large drawdown to compensate for the low permeability, the large pressure gradients seen in the reservoir and corresponding gas property changes caused by this cannot be ignored in the analysis. Observing this shortcoming in pressure buildup analysis of gas wells, Agarwal (1979) proposed the use of a real gas pseudotime, t_a^*, defined as

$$t_a^* = \int_0^t \frac{dt}{\mu(t)c_t(t)}. \quad \text{.....(2.22)}$$

Agarwal (1979) noted that while this is not a rigorous mathematical formulation (as is the case for pseudopressure, Eq. 2.4), it does improve the accuracy of the analysis. While Agarwal (1979) evaluated the changing viscosity and system compressibility at the wellbore, Fraim and Wattenbarger (1987) found that in a depleting reservoir, these parameters should be evaluated at the average reservoir pressure, and formulated the pseudotime in a slightly different way,

$$t_a = (\phi\mu c_t)_i \int_0^t \frac{dt}{\phi\left(\bar{p}\right)\mu\left(\bar{p}\right)c_t\left(\bar{p}\right)}. \quad \text{.....(2.23)}$$

Here, $\bar{p}$ is the average pressure in the reservoir, which is changing with time. Eq. 2.23 also accounts for changes in the pore volume, which are assumed to follow

$$\phi(p) = \phi_i \, \mathrm{e}^{-c_f(p_i - p)}. \quad \text{.....(2.24)}$$

When using pseudotime during transient flow, Anderson and Mattar (2005) suggest to use corrected pseudotime, where Eq. 2.23 is evaluated at the average pressure in the region of investigation, as defined by the DOI concept. The corrected pseudotime is the definition of pseudotime used in this work, and the terms corrected pseudotime and pseudotime will be used interchangeably. Anderson and Mattar (2005) also point out that evaluating fluid properties at a single average pressure might not be representative of the range of fluid properties observed throughout the reservoir, especially in the presence of large pressure gradients, but failing to apply a correction for the gas's pressure dependence will make accurate modeling of gas reservoirs impossible when applying solutions designed for slightly

compressible fluids. The effect of using pseudotime can be seen by substituting Eq. 2.23 for time in Eq. 2.6, which yields a dimensionless time that accounts for the pressure dependent parameters,

$$t_{Dxf} = \frac{0.00633k}{x_f^2}\int_0^t \frac{dt}{\phi\left(\bar{p}\right)\mu\left(\bar{p}\right)c_t\left(\bar{p}\right)}. \quad \text{.....(2.25)}$$

When the flow rate varies, Clarkson and Beierle (2010) recommend that pseudotime is included in the calculation of the linear superposition time as

$$t_{a,LS} = \sum_{j=1}^{n} \frac{\left(q_j - q_{j-1}\right)}{q_n}\sqrt{t_{a,n} - t_{a,j-1}}. \quad \text{.....(2.26)}$$

2.4.1 Adsorption

In shale reservoirs and other reservoirs high in organic content, the reservoir fluids are stored both as free fluid in the pores and in a sorbed state. Sorption is a general term that refers to adsorption and absorption, where adsorption is the accumulation of fluids on the surface area of the porous reservoir rock, and absorption refers to fluids being stored inside the organic reservoir material.

This study will focus on sorption by way of adsorption in shale gas reservoirs. The amount of adsorbed gas depends on properties such as pore size, specific surface area, pressure, temperature, and sorption affinity (Deahy-Dios et al., 2011). Several formulations have been proposed to model adsorption. In microporous media (pore diameter not exceeding 2 nm), Sing et al. (1985) recommend using a Type I isotherm such as the Langmuir isotherm (Langmuir, 1918), which has been found to adequately describe the adsorption process in shale reservoirs (Bump and McKee 1988). The Langmuir isotherm describes the volume of gas adsorbed on the reservoir rock at a given pressure under isothermal conditions, and can be formulated as

$$V_a = V_L \frac{p}{p + p_L}, \quad \text{.....(2.27)}$$

where V_a is the amount of adsorbed gas in scf per ton of reservoir rock, V_L (Langmuir volume) is the maximum adsorption capacity of the reservoir rock at a given temperature, in scf/ton, p is pore pressure, and p_L is the Langmuir pressure, both given in psia. As can be seen from Eq. 2.27, when the pore pressure is equal to the Langmuir pressure, the reservoir rock has

adsorbed half of its maximum adsorption capacity. **Fig. 2.5** shows the Langmuir curve for V_L = 100 scf/ton and p_L = 1000 psia, which are the base case values used in this study.

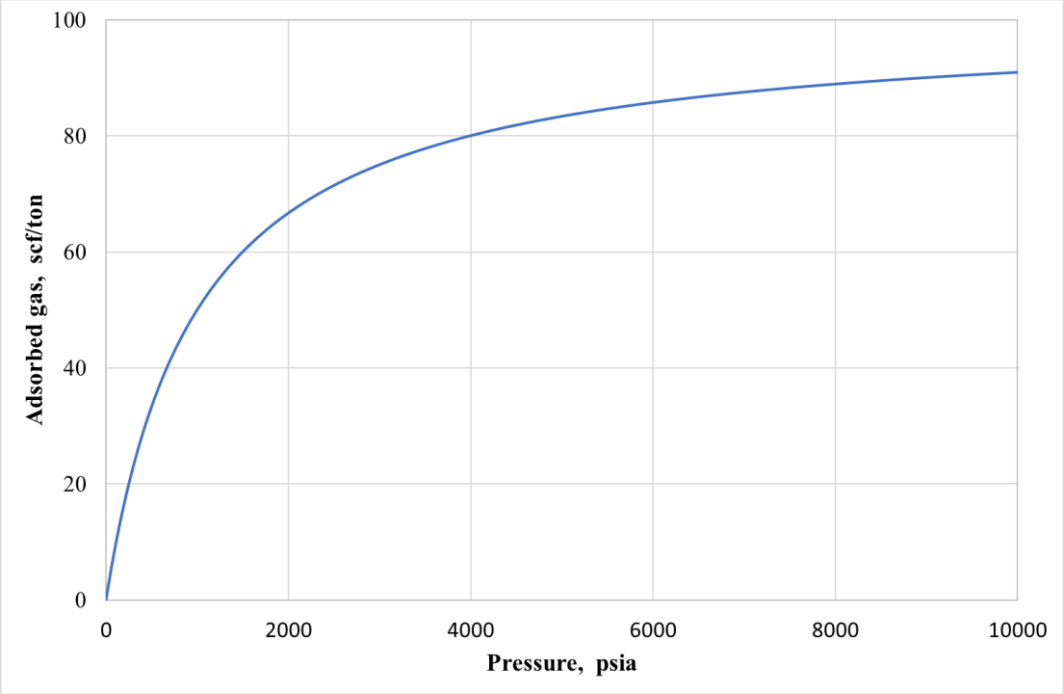

Fig. 2.5 - Langmuir curve, adsorbed gas as a function of pressure.

As pore pressure decreases, gas is desorbed (the opposite process of adsorption) from the rock and released into the pores as free gas. The increase of free gas caused by the desorption process can be expressed as an increase in compressibility, so that the total compressibility of a fully gas saturated reservoir is given by (Bump and McKee, 1988)

$$c_t = c_g + c_f + c_d \quad \text{.....(2.28)}$$

Here, c_g is the gas compressibility, c_f is the pore compressibility and c_d is the adsorption compressibility,

$$c_d = \frac{B_g \rho_B V_L p_L}{32.0368(p_L + p)^2 \phi}, \quad \text{.....(2.29)}$$

all given in psi^{-1}. In Eq. 2.29, B_g is the gas formation volume factor given in ft^3/scf, and ρ_B is the bulk density of the reservoir rock in g/cm^3. Adsorption will therefore play a role in the calculation of pseudotime through the modified total compressibility, but will not affect the pseudopressure calculation. The pseudotime and pseudopressure functions can be modified to account for other instances of complex reservoir behavior such as non-static permeability and non-Darcy flow (Clarkson, 2013), but these occurrences will not be investigated in this study.

2.5 Calculation of Pseudotime

The following three sections contain methods of correcting for pressure dependent rock and fluid parameters found in the dimensionless time expression, and are derived for infinite acting linear gas flow in the reservoir model shown in Fig. 2.1.

2.5.1 The Modified Ibrahim and Wattenbarger Method

In this work, an empirical modification suggested by Nystad (2015) is used to apply the correction factor proposed by Ibrahim and Wattenbarger (2005, 2006) to varying pressure data.

Ibrahim and Wattenbarger (2005, 2006) observed that under constant pressure production the square root of time plot deviates from its analytical value, causing an overestimation in the linear flow parameter calculated from the plot slope. They recommend to multiply the slope of the plot with an empirical correction factor,

$$f_{CP,IW} = 1 - 0.0852 D_D - 0.0857 D_D^2, \quad (2.30)$$

where D_D is the dimensionless drawdown, defined as

$$D_D = \frac{\left(p_p(p_i) - p_p(p_{wf})\right)}{p_p(p_i)}. \quad (2.31)$$

The subscript *IW* in Eq. 2.30 refers to the authors names. Nystad (2015) showed that this correction factor can also be applied to the LFDP for both constant and varying pressure data by evaluating the dimensionless drawdown at the flowing pressure at time *t* and using this to calculate a correction factor for each timestep. Eq. 2.30 and Eq. 2.31 are thus recast as functions of time;

$$f_{CP}^*(t) = 1 - 0.0852 D_D(t) - 0.0857 \left(D_D(t)\right)^2 \quad (2.32)$$

and

$$D_D^*(t) = \frac{\left(p_p(p_i) - p_p(p_{wf}(t))\right)}{p_p(p_i)}. \quad (2.33)$$

Nystad (2015) used the time dependent correction factor by multiplying Eq. 2.13 and Eq. 2.32 to form a corrected linear superposition time,

$$t_{LS}^{*} = f_{CP}^{*}(t_n)\sum_{j=1}^{n}\frac{\left(q_j - q_{j-1}\right)}{q_n}\sqrt{t_n - t_{j-1}}, \quad \text{.....(2.34)}$$

and used this as the abscissa plotting term in the LFDP, which is the formulation used in this work. For constant pressure production, applying Eq. 2.34 to correct the data is equivalent to correcting the LFDP slope with Eq. 2.30, but offers the advantage of visual inspection of the resulting correction, as the correction factor in applied through the plotting term instead of being multiplied with the uncorrected plot slope. For constant rate production Eq. 2.34 can be written as $t_{LS}^{*} = f_{CP}^{*}(t)\sqrt{t}$.

2.5.2 The Nobakht and Clarkson Method

This method of calculating pseudotime was proposed by Nobakht and Clarkson (2011a, 2011b, 2011c) for constant pressure, constant rate and varying rate and pressure production, respectively. Nobakht et al. (2011) extended the analysis method to include adsorption and gas slippage. A material balance equation[1] accounting for adsorption and formation compressibility is used,

$$\frac{\bar{p}}{\bar{Z}^{*}} = \frac{p_i}{Z^{*}}\left(1 - \frac{G_p}{G}\right), \quad \text{.....(2.35)}$$

where G_p and G are given in scf and are the produced gas and contacted gas in place, respectively. The contacted gas in place is the amount of gas, including adsorbed gas, initially in place within the region defined by the DOI at a given time. $\bar{Z}^{*}$ is the modified gas deviation factor, evaluated at the average pressure in the region determined by the DOI. Z^{*} is defined for a fully gas saturated reservoir (King, 1993) as

$$Z^{*} = \frac{Z}{e^{-c_f(p_i - p)} - \dfrac{\rho_B B_g V_L p}{32.0368(p_L + p)\phi}}. \quad \text{.....(2.36)}$$

The contacted gas in place at a given time in Eq. 2.35 is estimated with a drainage area of $4x_f \cdot y_{inv}$, which yields

[1] Nobakht and Clarkson (2011a, 2011b, 2011c) and Nobakht et al. (2011) used a scaled version of the King (1993) deviation factor proposed by Moghadam et al. (2011), Z^{**}, which is related to the King (1993) deviation factor by the relationship $Z^{**} = Z^{*}(Z_i/Z^{*}_i)$. As $Z_i^{**} = Z_i$, this scaling is will yield more intuitive values for the modified deviation factor, which could be an advantage when plotted, but will not otherwise change the material balance analysis (Moghadam et al 2011). Because of its simpler formulation, the King (1993) material balance equation is used in this study.

$$G = \frac{Ah\phi_i S_{gi}}{B^*_{gi}} = \frac{4x_f y_{inv} h\phi_i S_{gi}}{B^*_{gi}}, \quad \text{.....(2.37)}$$

where B^*_{gi} is a modified formation volume factor,

$$B^*_g = 0.0282 \frac{TZ^*}{p}, \quad \text{.....(2.38)}$$

that accounts for the adsorbed gas in place through the modified gas deviation factor. Using Eq. 2.21 and Eq. 2.38, the contacted gas in place can be expressed as

$$G = \frac{4\alpha h\varphi S_{gi} x_f \sqrt{k}}{B^*_{gi}\sqrt{(\varphi\mu c_t)_i}}\sqrt{t}, \quad \text{.....(2.39)}$$

which can be inserted into Eq. 2.35 to form

$$\frac{\bar{p}}{\bar{Z}^*} = \frac{p_i}{Z^*}\left(1 - \frac{B^*_{gi}\sqrt{(\varphi\mu c_t)_i}\,G_p}{4\alpha h\varphi S_{gi} x_f \sqrt{k}\sqrt{t}}\right). \quad \text{.....(2.40)}$$

It is important to note that the modified parameters denoted with an asterisk in Eqs. 2.35 through 2.40 are simply a practical means of inserting new variables in the equations, and does not change the physical meaning of their unmodified counterparts.

2.5.2.1 Constant Rate Production

Nobakht and Clarkson (2011b) showed that for constant rate production, under some simplifying assumptions, the early time slope of the LFDP can be used to get a good estimate of the linear flow parameter without the use of pseudotime. Nobakht and Clarkson (2011b) used this estimated linear flow parameter together with α = 0.113 to approximate the average pressure in the region of investigation at different times from

$$\frac{\bar{p}}{\bar{Z}^*} = \frac{p_i}{Z^*}\left(1 - \frac{B^*_{gi}\sqrt{(\varphi\mu c_t)_i}\,G_p}{4\cdot 0.113 h\varphi S_{gi} x_f \sqrt{k}\sqrt{t}}\right). \quad \text{.....(2.41)}$$

These average pressures were used to evaluate the pseudotime, Eq. 2.23, and a new LFDP using these pseudotimes was generated. Using the early time slope of the new LFDP to get a better estimate of the linear flow parameter, this procedure was repeated until convergence.

2.5.2.2 Constant Flowing Pressure Production

It was shown by Nobakht and Clarkson (2011a) that during constant pressure production, the average pressure within the distance of investigation is constant. Because of this property, the pseudotime, Eq. 2.23, takes the form

$$t_{a,CP} = \frac{(\varphi\mu c_t)_i}{\varphi\left(\bar{p}\right)\mu\left(\bar{p}\right)c_t\left(\bar{p}\right)}t. \quad \text{.....(2.42)}$$

With this linear relationship between pseudotime and time for constant pressure production, Nobakht and Clarkson (2011a) showed that a correction factor[2],

$$f_{CP} = \sqrt{\frac{(\varphi\mu c_t)_i}{\varphi\left(\bar{p}\right)\mu\left(\bar{p}\right)c_t\left(\bar{p}\right)}}, \quad \text{.....(2.43)}$$

can be defined, so that when the slope of a square root of time plot (or a LFDP) is multiplied by this correction factor, it corrects the data in the same way as using pseudotime, through the relationship $t_{a,CP} = f_{CP}^2 t$. Eq. 2.43 is analogous to the correction factor proposed by Ibrahim and Wattenbarger (2005, 2006), Eq. 2.30, which is a function of the pseudopressures evaluated at the initial and wellbore flowing pressures. The pseudopressure is affected by gas viscosity and gas compressibility (through the gas deviation factor), but will not be influenced by changing values of desorption compressibility and formation compressibility. Desorption compressibility and formation compressibility are thus not included in Eq. 2.30, but are accounted for in Eq. 2.43.

Using Eq. 2.19 and assuming that there is no skin factor, the cumulative gas production can be expressed as

$$G_p = \int_o^t q dt = \frac{2\sqrt{t}\left(p_p(p_i) - p_p(p_{wf})\right)}{m_{CP} f_{CP}}. \quad \text{.....(2.44)}$$

Substituting Eqs. 2.20, 2.38, and 2.44 into Eq. 2.40 and using an empirically obtained DOI constant with a value of 0.203, Nobakht and Clarkson (2011a) showed that the average pressure in the region of investigation can be expressed by

[2] Changes in porosity were not included in the correction factor proposed by Nobakht and Clarkson (2011a). This simplification is often used, as porosity changes can be seen as neglectable when compared to changes in gas compressibility.

$$\frac{\bar{p}}{\bar{Z}^*} = \frac{p_i}{Z^*}\left(1 - 0.220\frac{\left(Z^*\mu_g c_t\right)_i\left(p_p(p_i) - p_p(p_{wf})\right)}{S_{gi}\, p_i\, f_{CP}}\right). \quad \text{.....(2.45)}$$

This equation can be solved for the average pressure, from which the correction factor, Eq. 2.43, can be evaluated and used to correct the plot slope. Alternatively, the average pressure found from Eq. 2.45 can be used to evaluate the pseudotime, so that the correction is incorporated into the plotting term of the LFDP. The latter method is used in this study, as it allows for visual inspection of the correction on the LFDP.

2.5.2.3 Variable Rate and Flowing Pressure Production

Nobakht and Clarkson (2011c) propose to calculate pseudotime for variable rate and variable pressure production in the following way: from the early time slope of a square root of (regular) time plot of the data, the linear flow parameter is calculated for both the constant rate assumption, Eq. 2.16, and the constant pressure assumption, Eq. 2.20. Nobakht and Clarkson (2011c) suggest to compare these two estimates to the linear flow parameter calculated from the LFDP (i.e. Eq. 2.16 where the early time slope is taken from a plot using superposition with regular time) and correct the data with the constant rate approach outlined previously if the linear flow parameter calculated from the LFDP is closer to the estimate from the constant rate assumption than the estimate from the constant pressure assumption. If the opposite is the case, Nobakht and Clarkson (2011c) recommend using

$$\frac{\bar{p}}{\bar{Z}^*} = \frac{p_i}{Z^*}\left(1 - \frac{B^*_{gi}\sqrt{\left(\varphi\mu c_t\right)_i}\, G_p}{4 \cdot 0.159 h\varphi S_{gi} x_f \sqrt{k}\sqrt{t}}\right), \quad \text{.....(2.46)}$$

which is Eq. 2.40 where a DOI constant value of 0.159 is used, together with the methodology outlined in the constant rate section.

2.5.3 The Modified Behmanesh Method

In this work, an empirical modification is proposed to the correction technique developed for constant pressure production by Behmanesh (2016), to make the methodology applicable to varying pressure data.

Behmanesh (2016) showed that under constant pressure production, the average pseudopressure in the region of influence can be expressed as a weighted arithmetic mean value of the pseudopressures at initial and wellbore conditions. With the distance of

investigation defined by Eq. 2.21, $\alpha = 0.194$, the average pseudopressure within this distance is constant, and given by Behmanesh (2016) as

$$p_p(\bar{p}) = 0.56\,p_p(p_i) + 0.44\,p_p(p_{wf}). \quad \text{.....(2.47)}$$

For constant pressure production, the pseudotime used in the LFDP analysis is evaluated at the average pressure found from Eq. 2.47.

The author proposes that a modified version of Eq. 2.47 can be applied to varying pressure production data. The average pseudopressure in the region of investigation at a given time is approximated as

$$p_p(\bar{p}(t)) = 0.56\,p_p(p_i) + 0.44\,p_p(p_{wf}(t)), \quad \text{.....(2.48)}$$

and a correction factor originally derived for constant pressure production is evaluated at the corresponding average pressure,

$$f_{CP}^{**}(t) = \sqrt{\frac{(\varphi\mu c_t)_i}{\varphi\left(\bar{p}(t)\right)\mu\left(\bar{p}(t)\right)c_t\left(\bar{p}(t)\right)}}. \quad \text{.....(2.49)}$$

The motivation for this modification is to use the constant pressure formulation derived by Behmanesh (2016) in the same way as was done with the Ibrahim and Wattenbarger (2005, 2006) correction factor by Nystad (2015), by defining a new corrected linear superposition time as

$$t_{LS}^{**} = f_{CP}^{**}(t_n)\sum_{j=1}^{n}\frac{\left(q_j - q_{j-1}\right)}{q_n}\sqrt{t_n - t_{j-1}}, \quad \text{.....(2.50)}$$

and using it in the LFDP analysis for varying pressure data. Correcting the data with Eq. 2.50 during constant pressure production is equivalent to evaluating the pseudotime at the average pressure found from Eq. 2.48. For constant rate production Eq. 2.50 can be written as $t_{LS}^{**} = f_{CP}^{**}(t)\sqrt{t}$.

3 Analysis of Simulated Production Data

To test the applicability of the linear flow diagnostic plot as a tool to extract reservoir parameters from production data, a series of numerical simulations modeling linear flow in the reservoir geometry shown in Fig. 2.1 were performed with the numerical simulator Sensor. The investigated permeability range is 0.001 – 0.00001 md (10 – 1000 nd), to represent a shale reservoir. All simulation cases were analyzed with the LFDP, and the slope of the plot was used together with the input simulation parameters to extract the fracture half-length from Eq. 2.16. For each simulated dataset, the linear superposition time was calculated in the four following ways:

(1) Pseudotime and correction factors were not used. The linear superposition time was calculated from Eq. 2.13.
(2) The data was corrected with the modified Ibrahim and Wattenbarger method, Eq. 2.34, as outlined in section 2.5.1.
(3) The method proposed by Nobakht and Clarkson, as described in section 2.5.2, was used to calculate the pseudotime used to evaluate Eq. 2.26.
(4) The modified Behmanesh method proposed in this work, section 2.5.3, was applied to correct the data by use of Eq. 2.50.

All simulations, unless otherwise specified, were performed for a duration of two years with the base case parameters given in **Table 2.**

Table 2 - Base case parameters used in numerical simulation runs.

Base case parameters		
Parameter	**Value**	**Unit**
x_f	300	ft
x_e	300	ft
y_e	1500	ft
h	200	ft
φ_i	0.05	fraction
S_g	1	fraction
SG	0.65	air = 1
p_L	1000	psia
F_c	1000	md-ft
s	0	dim.less

3.1 Constant Flowing Pressure Production

30 simulated cases were run with the constant flowing pressure boundary condition. The simulation parameters and the results from the LFDP analysis are summarized in **Table 3**. The analysis results presented in Table 3 are shown in **Figs 3.1 through 3.3**. The LFDP from simulation cases no. 2, 21, 17 and 30* are shown in **Figs 3.4 through 3.7**, respectively, together with the analytical slope calculated from the input simulation parameters.

Table 3 - Simulation parameters and results from the LFDP analysis on constant pressure data.

Simulation parameters									Analysis results			
									(1)	(2)	(3)	(4)
Case no.	p_i psia	p_{wf} psia	k 10^{-6}md	c_f psi^{-1}	c_{ti} psi^{-1}	μ_{gi} cP	V_L scf/ton	T °F	x_f ft	x_f ft	x_f ft	x_f ft
1	10000	1000	1000	5.0E-06	3.6E-05	0.044	0	120	394	329	308	311
2	10000	1000	100	5.0E-06	3.6E-05	0.044	0	120	394	330	309	311
3	10000	1000	10	5.0E-06	3.6E-05	0.044	0	120	396	331	310	312
4	5000	500	1000	5.0E-06	1.1E-04	0.030	0	120	385	321	300	300
5	5000	500	100	5.0E-06	1.1E-04	0.030	0	120	386	321	300	301
6	5000	500	10	5.0E-06	1.1E-04	0.030	0	120	388	323	301	302
7	2000	200	1000	5.0E-06	5.4E-04	0.017	0	120	341	284	306	306
8	2000	200	100	5.0E-06	5.4E-04	0.017	0	120	342	284	307	307
9	2000	200	10	5.0E-06	5.4E-04	0.017	0	120	344	286	308	308
10	10000	1000	1000	5.0E-06	4.0E-05	0.044	100	120	402	337	311	313
11	10000	1000	100	5.0E-06	4.0E-05	0.044	100	120	403	337	311	313
12	10000	1000	10	5.0E-06	4.0E-05	0.044	100	120	404	338	312	314
13	5000	500	1000	5.0E-06	1.3E-04	0.030	100	120	395	329	304	305
14	5000	500	100	5.0E-06	1.3E-04	0.030	100	120	395	329	305	306
15	5000	500	10	5.0E-06	1.3E-04	0.030	100	120	398	331	306	307
16	2000	200	1000	5.0E-06	6.7E-04	0.017	100	120	364	303	313	313
17	2000	200	100	5.0E-06	6.7E-04	0.017	100	120	365	304	314	314
18	2000	200	10	5.0E-06	6.7E-04	0.017	100	120	367	305	315	316
19	5000	500	100	0E+00	1.1E-04	0.030	0	120	392	327	300	301
20	5000	500	100	5.0E-05	1.6E-04	0.030	0	120	344	286	301	302
21	10000	5000	100	5.0E-06	3.6E-05	0.044	0	120	332	308	297	297
22	5000	2500	100	5.0E-06	1.1E-04	0.030	0	120	345	313	296	296
23	2000	1000	100	5.0E-06	5.4E-04	0.017	0	120	322	287	299	299
24	5000	500	100	5.0E-06	1.4E-04	0.026	0	200	371	309	303	303
25	5000	500	100	5.0E-06	1.5E-04	0.025	0	300	363	303	305	306
26	5000	500	100	5.0E-06	1.4E-04	0.030	200	120	403	335	308	309
27	5000	500	100	5.0E-06	1.6E-04	0.030	300	120	409	340	311	312
28	5000	500	100	5.0E-06	1.7E-04	0.030	400	120	413	344	313	314
29*	5000	500	100	5.0E-06	1.3E-04	0.030	100	120	421	351	328	328
30*	2000	200	100	5.0E-06	6.7E-04	0.017	100	120	406	337	364	364

(1) No correction factor is used in the analysis.
(2) The Ibrahim and Wattenbarger correction factor is used in the analysis.
(3) The Nobakht and Clarkson correction factor is used in the analysis.
(4) The Behmanesh correction factor is used in the analysis.
* The simulation case is analyzed ignoring the presence of adsorption.

Simulation cases 1 – 9 investigate varying initial pressures and permeabilities, where the flowing wellbore pressures are set to 10% of the initial pressures. Cases 10 – 18 include adsorption, but are otherwise a repetition of cases 1 – 9. Cases 19 – 28 are designed to study the effects of varying formation compressibility, drawdown, reservoir temperature and Langmuir volume. Cases 29* and 30* are the same as cases 14 and 17, respectively, but are analyzed with the assumption that there is no adsorption (i.e. the Langmuir volume is assumed to be equal to zero in the LFDP analysis), while the simulated data being analyzed is generated from a reservoir model that includes adsorption.

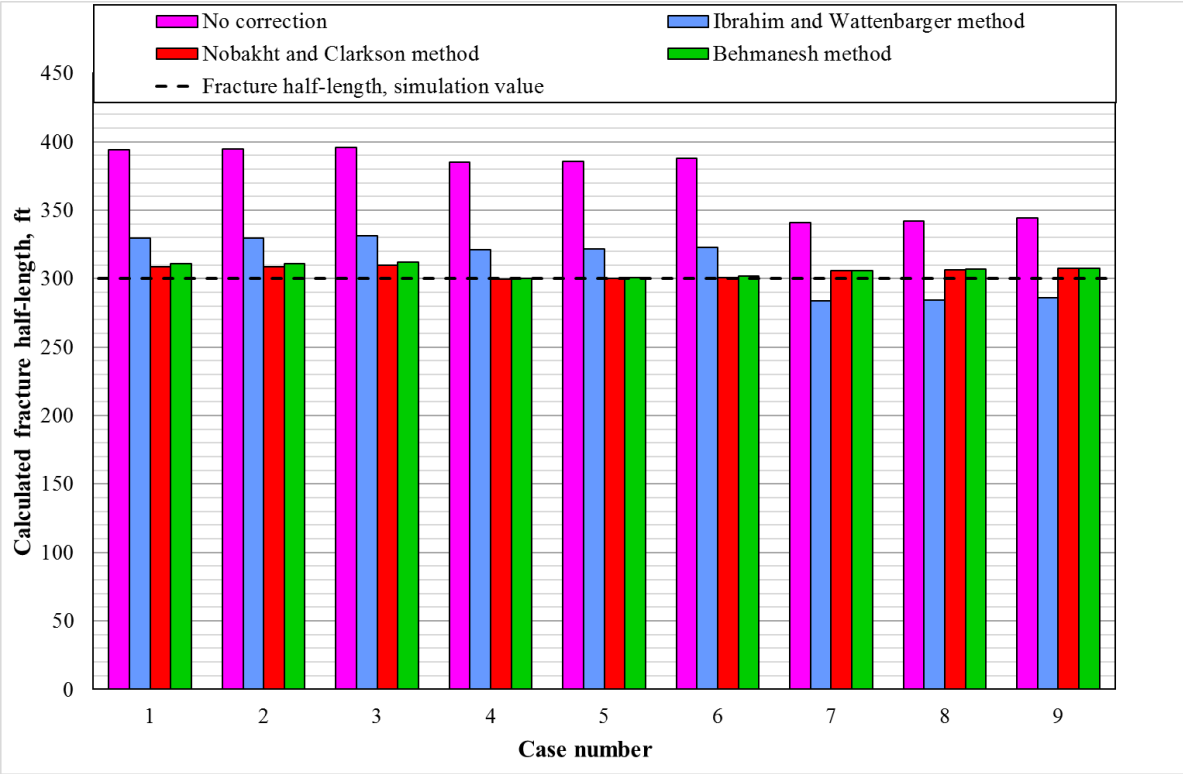

Fig. 3.1 - Calculated fracture half-lengths from the LFDP analysis on simulation cases 1 - 9.

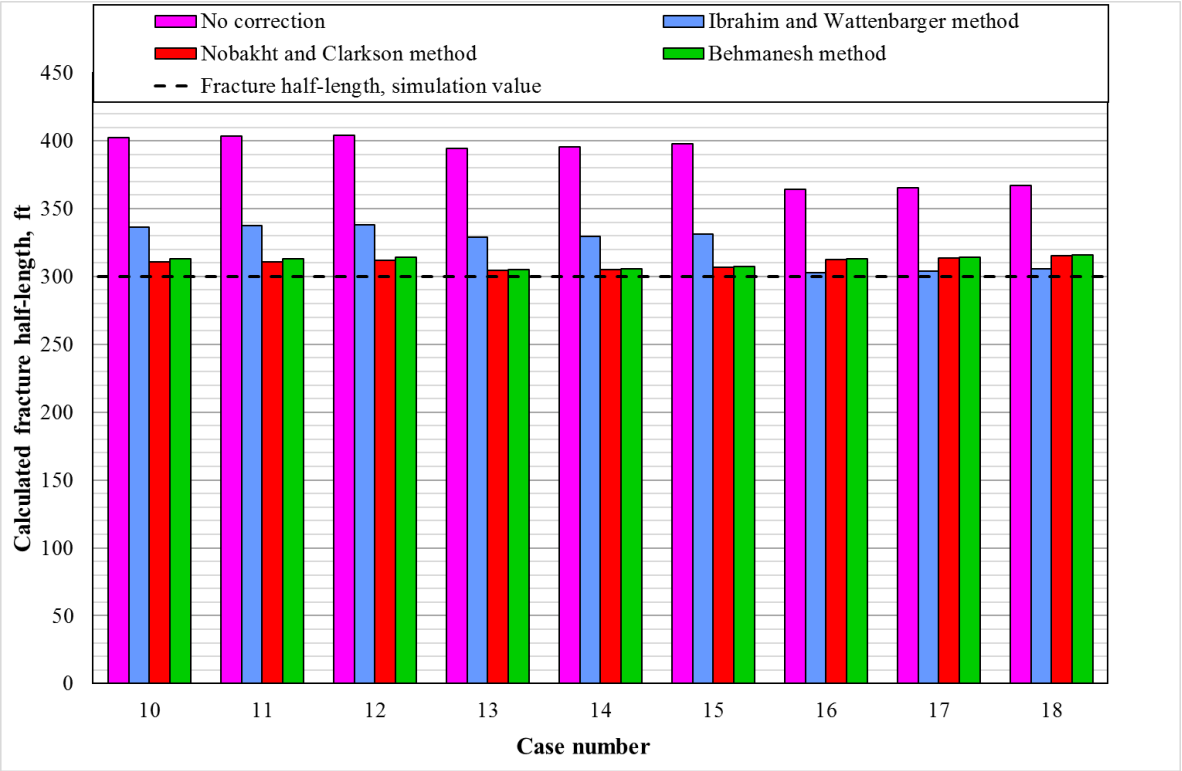

Fig. 3.2 - Calculated fracture half-lengths from the LFDP analysis on simulation cases 10 - 18.

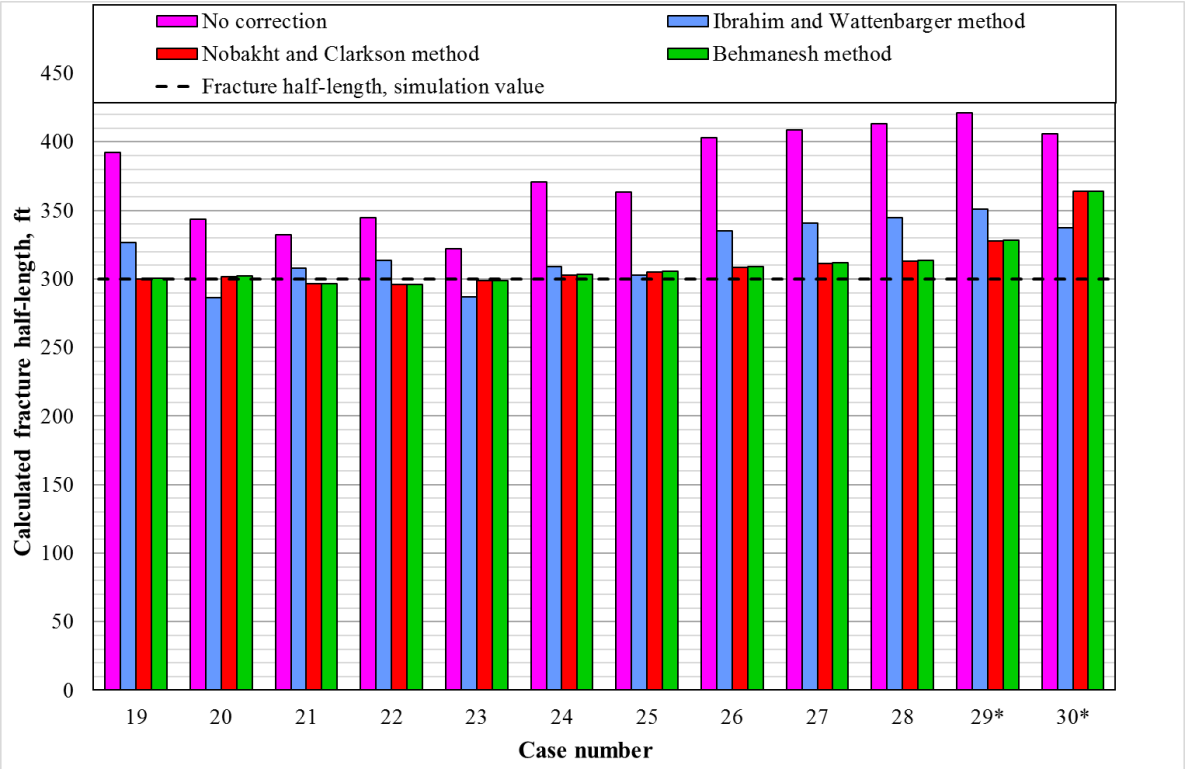

Fig. 3.3 - Calculated fracture half-lengths from the LFDP analysis on simulation cases 19 – 30. In simulation cases number 29* and 30*, the presence of adsorption in the simulated data is ignored in the LFDP analysis.

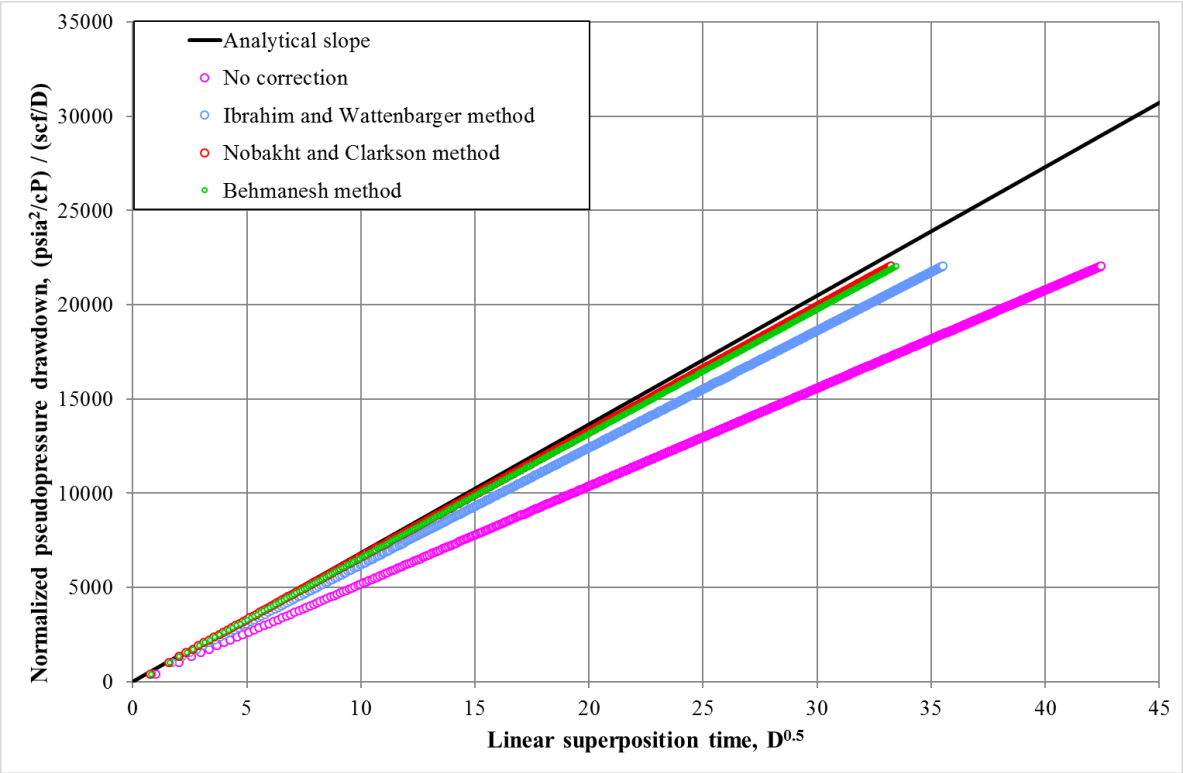

Fig. 3.4 - LFDP for simulation case no. 2.

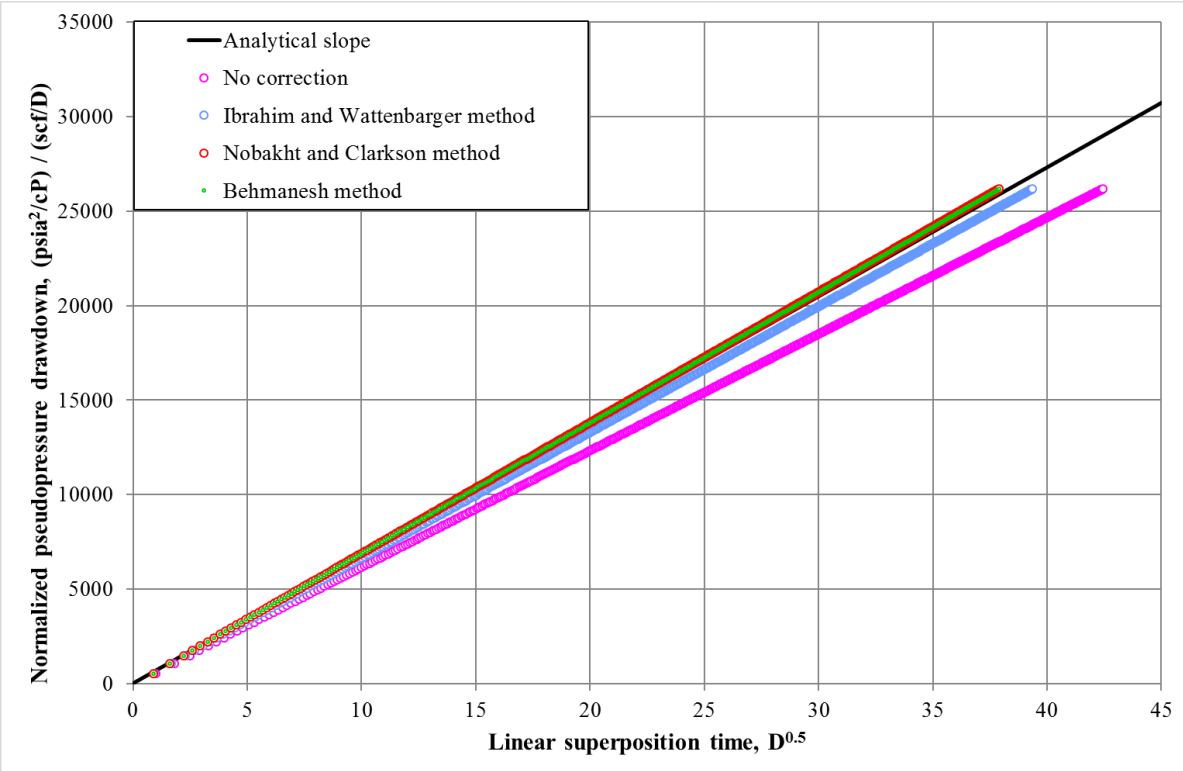

Fig. 3.5 - LFDP for simulation case no. 21. This case is equal to case no. 2, except for a smaller drawdown.

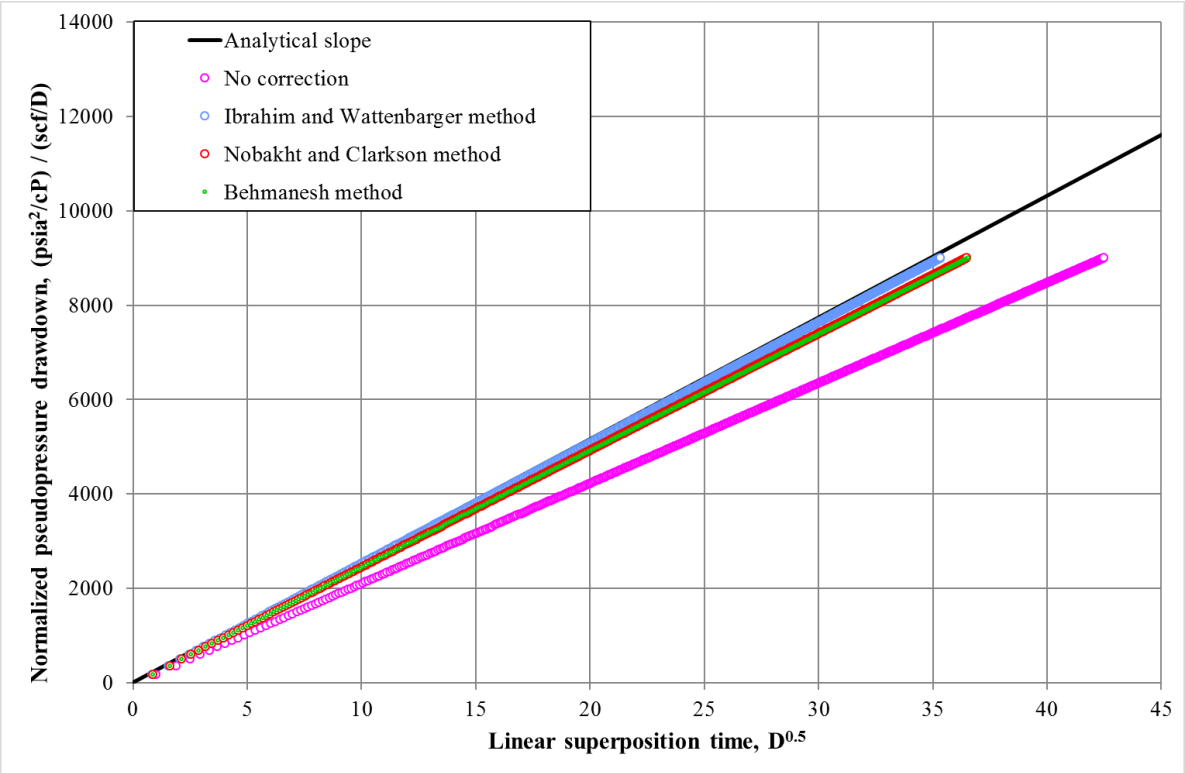

Fig. 3.6 - LFDP for simulation case no. 17.

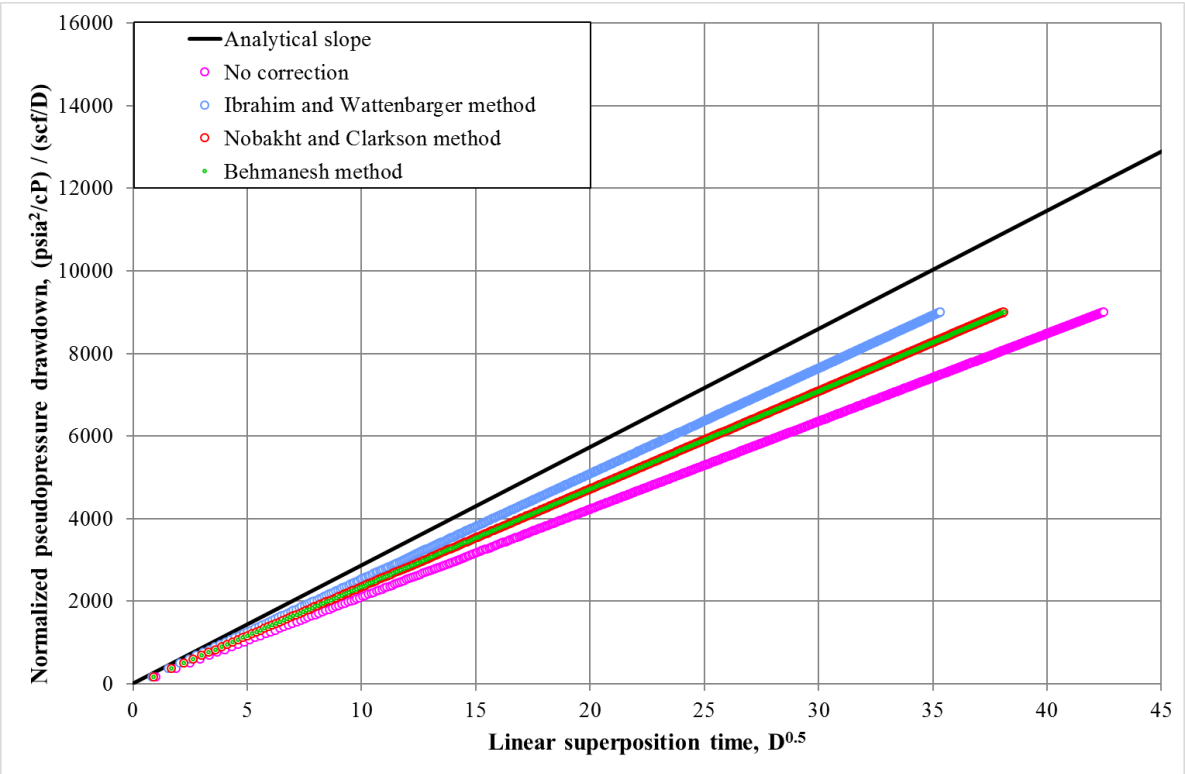

Fig. 3.7 - LFDP for simulation case no. 30*. This is the same simulated data as in case no. 17, but adsorption is assumed to not be present in the LFDP analysis (this includes the shown analytical slope, calculated with an assumed adsorption compressibility value of 0).

3.2 Constant Rate Production

To test the applicability of the previously described correction methods, 31 simulation runs were performed for the constant flow rate boundary condition. The results from the analysis are shown in **Table 4**, together with the simulation parameters used. The analysis results are presented in **Figs 3.8 through 3.10**, and the LFDP for simulation cases 32, 49, 58 and 61 are shown in **Figs 3.11 through 3.14**.

Table 4 - Simulation parameters and results from the LFDP analysis on constant rate data.

Simulation parameters									Analysis results			
									(1)	(2)	(3)	(4)
Case no.	p_i psia	q_g Mscf/D	k 10^{-6}md	c_f psi^{-1}	c_{ti} psi^{-1}	μ_{gi} cP	V_L scf/ton	T °F	x_f ft	x_f ft	x_f ft	x_f ft
31	10000	700	1000	5.0E-06	3.6E-05	0.044	0	120	311	307	300	299
32	10000	220	100	5.0E-06	3.6E-05	0.044	0	120	313	307	301	300
33	10000	70	10	5.0E-06	3.6E-05	0.044	0	120	317	310	303	302
34	5000	425	1000	5.0E-06	1.1E-04	0.030	0	120	315	309	301	299
35	5000	135	100	5.0E-06	1.1E-04	0.030	0	120	317	311	302	300
36	5000	43	10	5.0E-06	1.1E-04	0.030	0	120	323	315	304	302
37	2000	150	1000	5.0E-06	5.4E-04	0.017	0	120	306	292	300	299
38	2000	48	100	5.0E-06	5.4E-04	0.017	0	120	310	295	301	300
39	2000	15.2	10	5.0E-06	5.4E-04	0.017	0	120	315	295	303	302
40	10000	700	1000	5.0E-06	4.0E-05	0.044	100	120	312	307	301	299
41	10000	220	100	5.0E-06	4.0E-05	0.044	100	120	316	307	301	300
42	10000	70	10	5.0E-06	4.0E-05	0.044	100	120	318	311	303	302
43	5000	425	1000	5.0E-06	1.3E-04	0.030	100	120	317	310	301	299
44	5000	135	100	5.0E-06	1.3E-04	0.030	100	120	317	311	302	300
45	5000	43	10	5.0E-06	1.3E-04	0.030	100	120	323	315	304	302
46	2000	150	1000	5.0E-06	6.7E-04	0.017	100	120	314	301	302	301
47	2000	48	100	5.0E-06	6.7E-04	0.017	100	120	317	302	303	303
48	2000	15.2	10	5.0E-06	6.7E-04	0.017	100	120	322	304	307	306
49	10000	100	100	5.0E-06	3.6E-05	0.044	0	120	308	304	300	299
50	5000	70	100	5.0E-06	1.1E-04	0.030	0	120	313	308	301	299
51	2000	25	100	5.0E-06	5.4E-04	0.017	0	120	306	296	300	299
52	5000	70	100	0.0E+00	1.1E-04	0.030	0	120	313	309	301	299
53	5000	70	100	5.0E-05	1.6E-04	0.030	0	120	306	298	301	300
54	5000	70	100	5.0E-06	1.4E-04	0.026	0	200	312	306	301	299
55	5000	70	100	5.0E-06	1.5E-04	0.025	0	300	311	303	301	300
56	5000	135	100	5.0E-06	1.4E-04	0.030	200	120	313	309	302	301
57	5000	135	100	5.0E-06	1.7E-04	0.030	400	120	317	313	303	301
58*	5000	135	100	5.0E-06	1.3E-04	0.030	100	120	339	332	321	321
59*	2000	48	100	5.0E-06	6.7E-04	0.017	100	120	352	334	340	341
60**	5000	375	100	5.0E-06	1.1E-04	0.030	0	120	332	318	305	303
61**	5000	375	100	5.0E-06	1.3E-04	0.030	100	120	331	319	306	303

(1) Regular time (no correction) is used in the analysis.

(2) The modified Ibrahim and Wattenbarger method is used in the analysis.

(3) The Nobakht and Clarkson method is used in the analysis.

(4) The modified Behmanesh method is used in the analysis.

* The simulation case is analyzed ignoring the presence of adsorption.

**The simulation case in run for 100 days.

Simulation cases 31 – 39 investigate varying initial pressures and permeabilities, where the flow rate is chosen so that on the last day of simulation, the flowing wellbore pressure will be less than 10% of the initial reservoir pressure. Cases 40 – 48 include adsorption, but are otherwise a repetition of cases 31 – 39. Cases 49 – 57 investigate the effects of varying formation compressibility, flow rate, reservoir temperature and Langmuir Volume. Cases 58* and 59* are analyzed with the assumption that there is no adsorption (i.e. the Langmuir volume is assumed to be equal to zero in the LFDP analysis), while the simulated data being analyzed is generated from a reservoir model that includes adsorption. Cases 60** and 61** are run for 100 days, to accommodate a higher flow rate without the flowing pressures reaching their constraint (producing against atmospheric pressure).

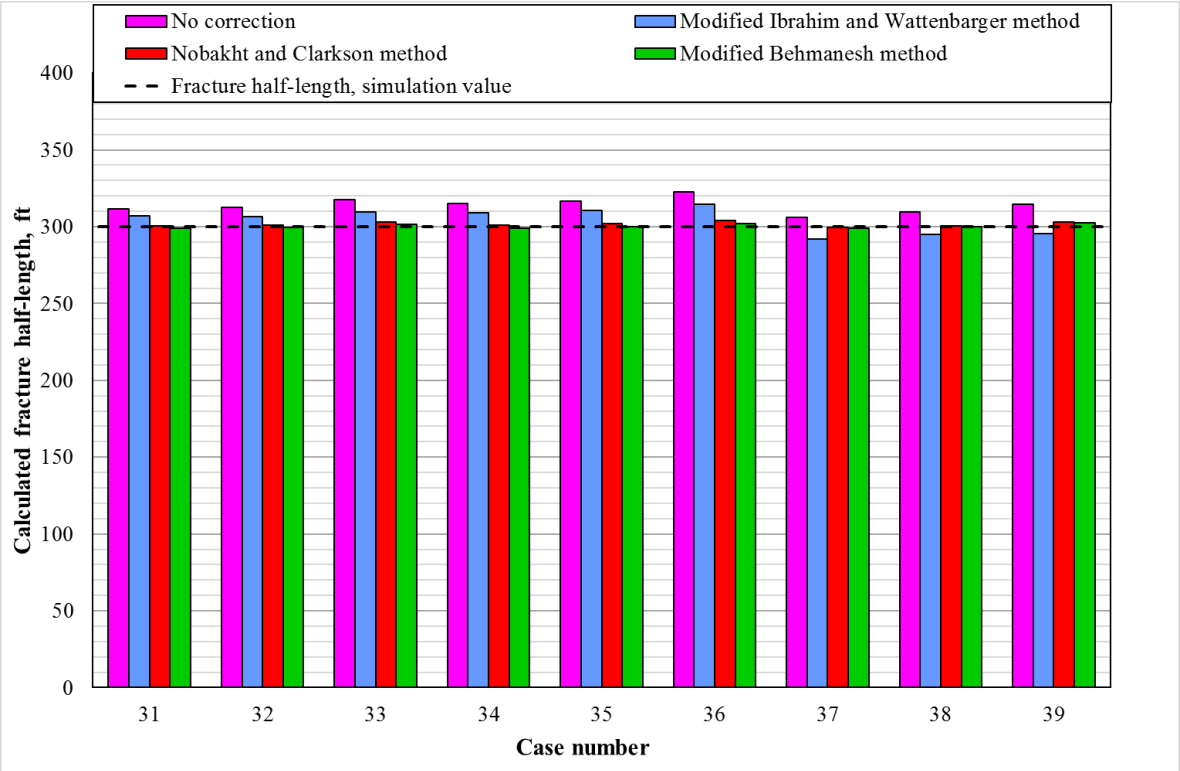

Fig. 3.8 - Calculated fracture half-lengths from the LFDP analysis on simulation cases 31 - 39.

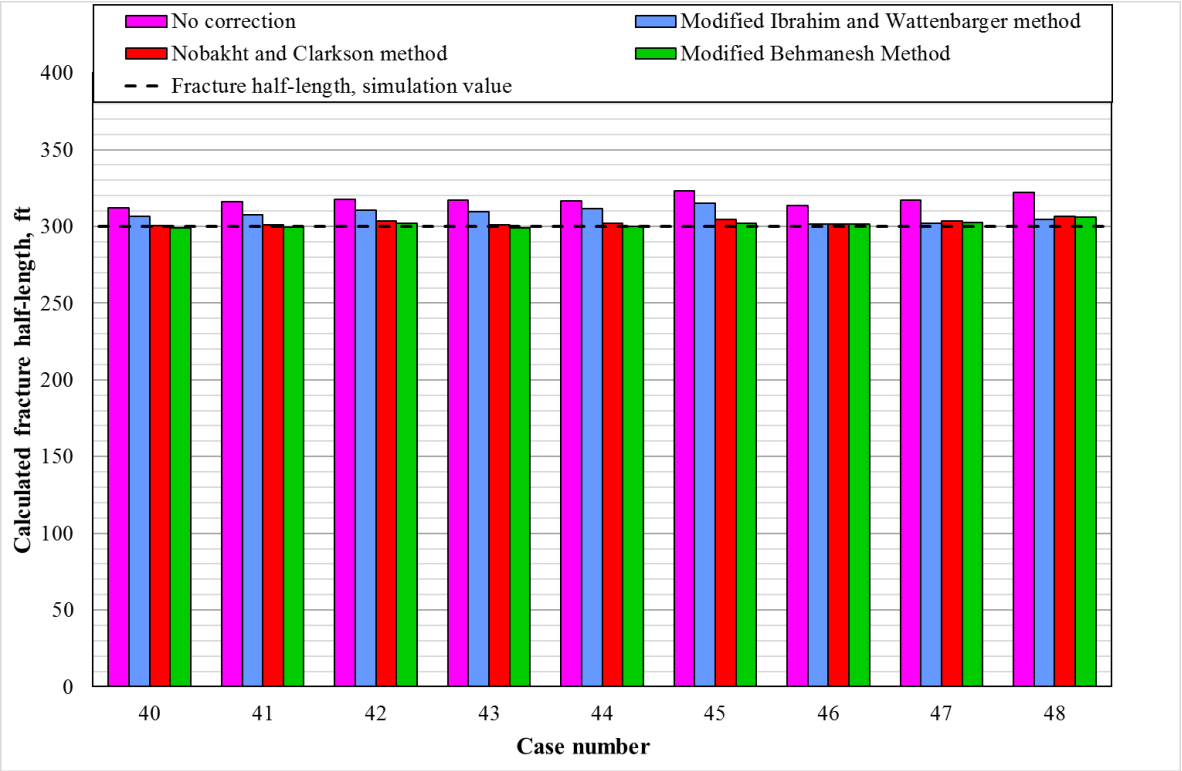

Fig. 3.9 - Calculated fracture half-lengths from the LFDP analysis on simulation cases 40 - 48.

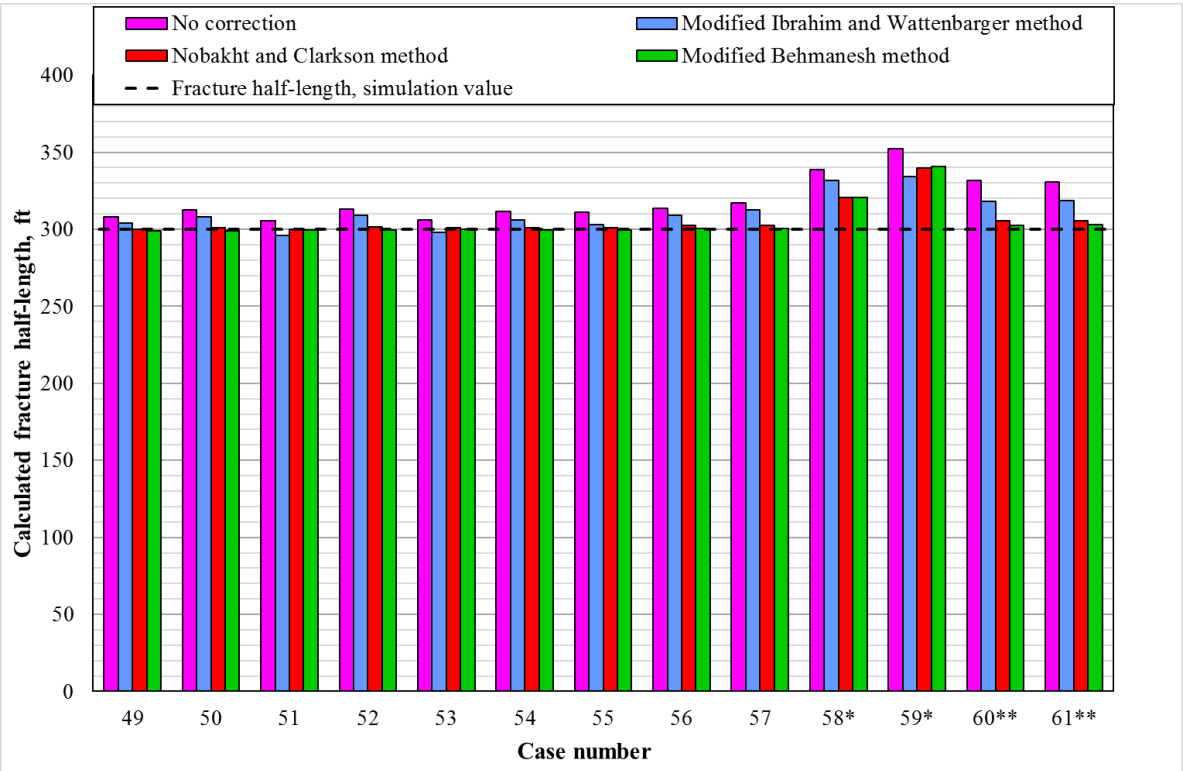

Fig. 3.10 - Calculated fracture half-lengths from the LFDP analysis on simulation cases 49 – 61. The analysis of case 58* and 59* has ignored the presence of adsorption in the data being analyzed. Simulation cases number 60 and 61** are run for 100 days.**

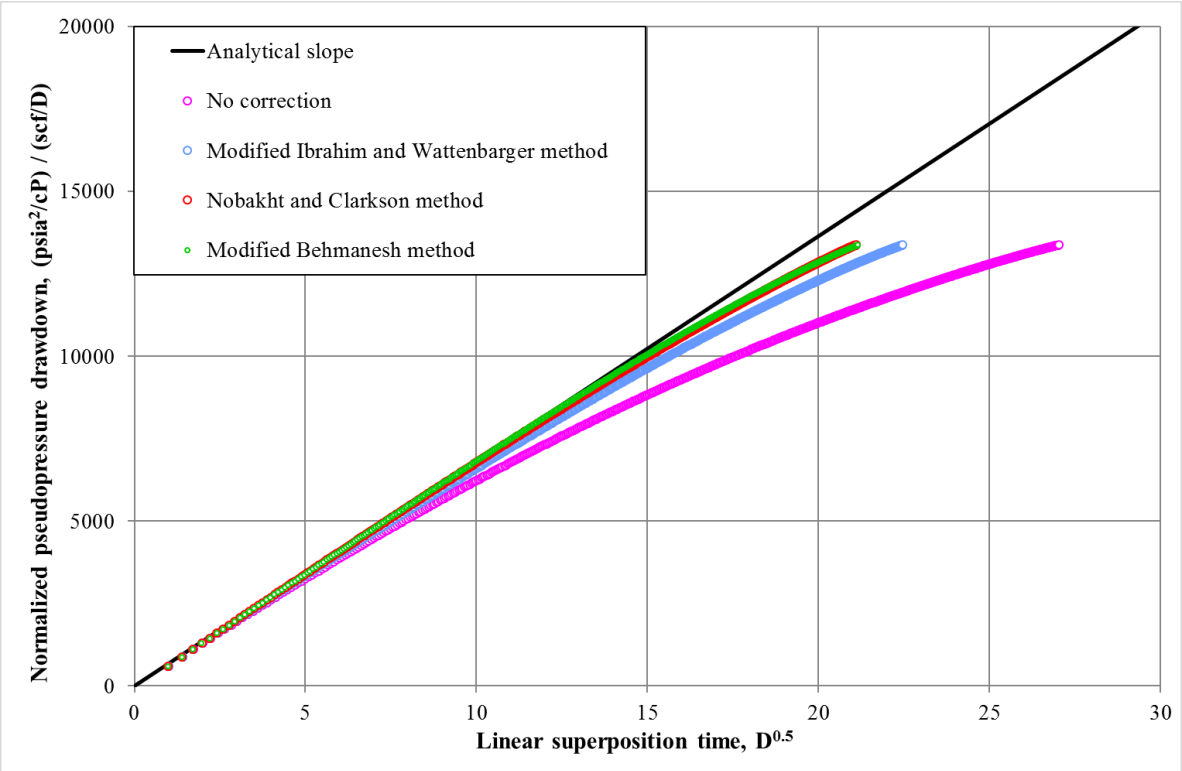

Fig. 3.11 - LFDP for simulation case no. 32.

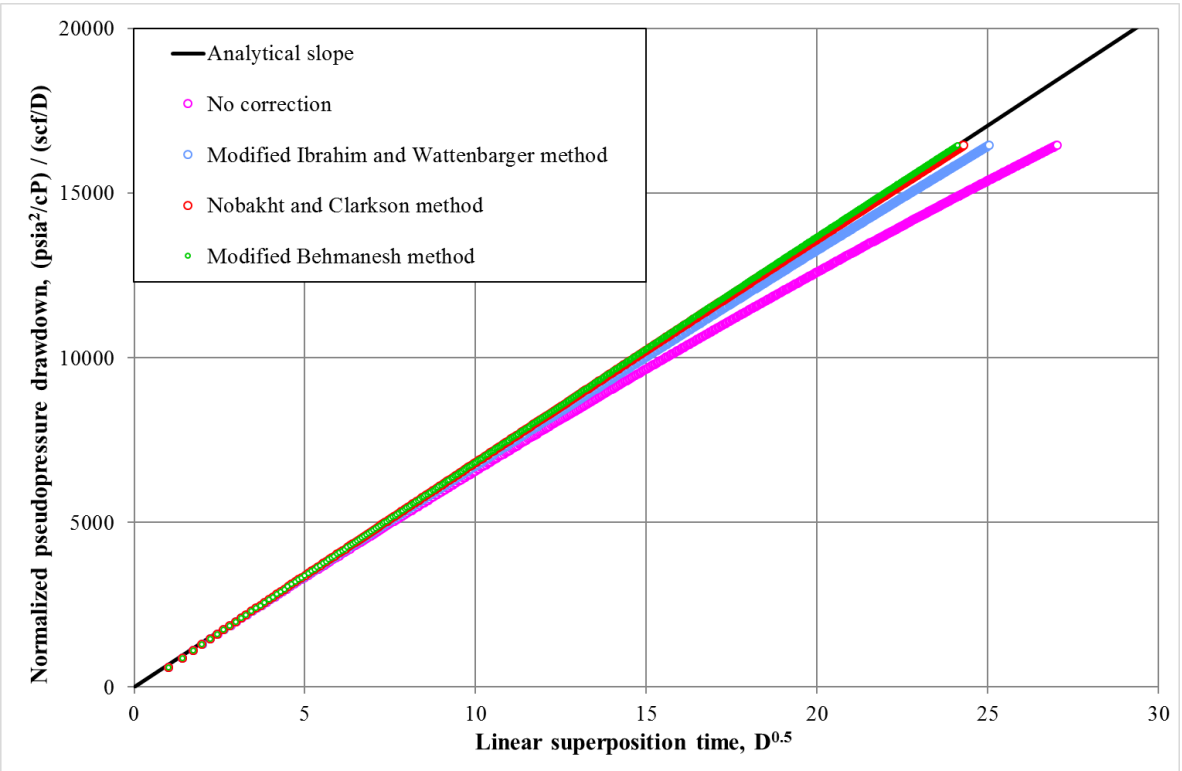

Fig. 3.12 - LFDP for simulation case no. 49. This case has the same parameters as case no. 32, except for a lower flow rate.

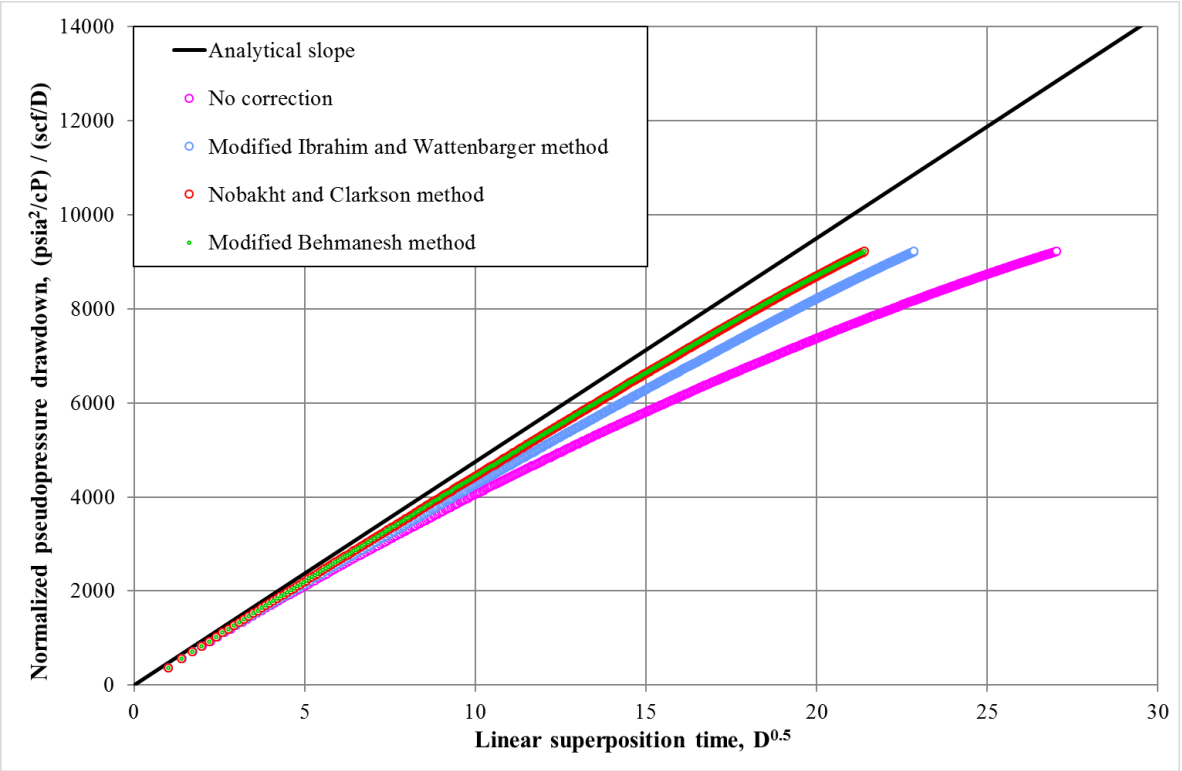

Fig. 3.13 - LFDP for simulation case no. 58*. Adsorption is included in the simulated data being analyzed, but adsorption is assumed to not be present in the LFDP analysis (this includes the shown analytical slope, calculated with an assumed adsorption compressibility value of 0).

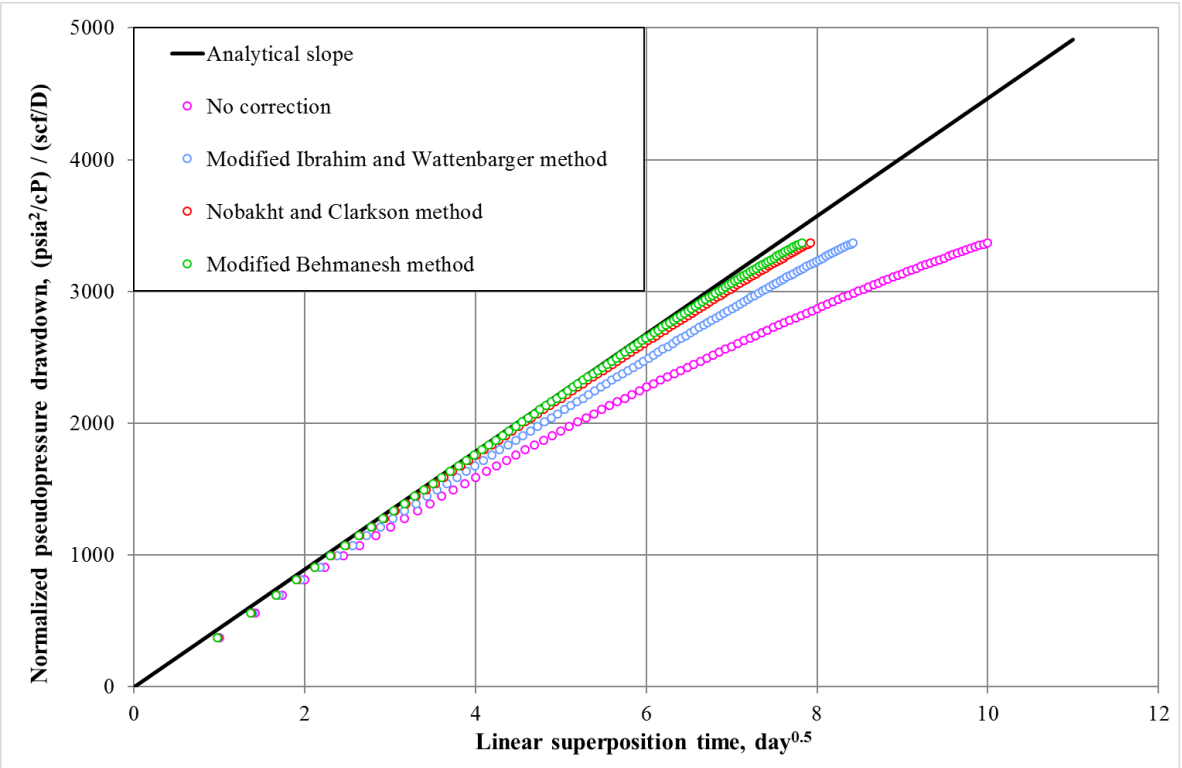

Fig. 3.14 - LFDP for simulation case no. 61*. The simulation is run for 100 days.

3.3 Variable Rate and Flowing Pressure Production

To investigate the performance of the analysis method for variable rate and flowing pressure, 24 simulation runs were performed. Four different pressure profiles were studied, with varying initial pressure, permeability, and Langmuir volume. In addition to the base case parameters given in Table 2, the following values were used for the variable rate and flowing pressure simulations: T = 120°F and c_f = 5E-6 psi^{-1}. The results of the investigation are presented in **Fig. 3.15** and **Fig. 3.16**, and in **Table 5** together with the simulation parameters. The column marked (0) in Table 5 signifies whether the constant rate or constant flowing pressure approach was determined to be applicable for the Nobakht and Clarkson method, as outlined in section 2.5.2.3. The LFDP for simulation cases 63, 68, 78 and 84 are shown in **Figs 3.17 through 3.24**, together with their corresponding rate and pressure profiles. The investigated pressure profiles are also shown together in **Fig. 3.25**.

Table 5 - Simulation parameters and results from the LFDP analysis on varying rate and flowing pressure data.

Case no.	p_i psia	p_{wf} psia	k 10^{-6}md	c_{ti} psi^{-1}	μ_{gi} cP	V_L scf/ton	(0) -	(1) x_f ft	(2) x_f ft	(3) x_f ft	(4) x_f ft
62	10000	Fig. 3.17	1000	3.6E-05	0.044	0	p_{const}	354	321	299	304
63	10000	Fig. 3.17	100	3.6E-05	0.044	0	p_{const}	359	320	299	304
64	10000	Fig. 3.17	10	3.6E-05	0.044	0	p_{const}	362	324	302	306
65	5000	Fig. 3.21	1000	1.1E-04	0.030	0	q_{const}	336	320	297	302
66	5000	Fig. 3.21	100	1.1E-04	0.030	0	q_{const}	339	319	294	303
67	5000	Fig. 3.21	10	1.1E-04	0.030	0	q_{const}	347	323	296	305
68	5000	Fig. 3.19	1000	1.1E-04	0.030	0	p_{const}	376	320	295	301
69	5000	Fig. 3.19	100	1.1E-04	0.030	0	p_{const}	381	320	294	301
70	5000	Fig. 3.19	10	1.1E-04	0.030	0	p_{const}	386	322	295	301
71	2000	Fig. 3.23	1000	5.4E-04	0.017	0	q_{const}	309	299	300	300
72	2000	Fig. 3.23	100	5.4E-04	0.017	0	q_{const}	310	304	302	302
73	2000	Fig. 3.23	10	5.4E-04	0.017	0	q_{const}	316	305	304	304
74	10000	Fig. 3.17	1000	4.0E-05	0.044	100	p_{const}	364	326	301	305
75	10000	Fig. 3.17	100	4.0E-05	0.044	100	p_{const}	363	321	300	304
76	10000	Fig. 3.17	10	4.0E-05	0.044	100	p_{const}	364	328	300	307
77	5000	Fig. 3.21	1000	1.3E-04	0.030	100	q_{const}	339	320	297	301
78	5000	Fig. 3.21	100	1.3E-04	0.030	100	q_{const}	338	323	299	303
79	5000	Fig. 3.21	10	1.3E-04	0.030	100	q_{const}	347	326	298	304
80	5000	Fig. 3.19	1000	1.3E-04	0.030	100	p_{const}	378	326	296	302
81	5000	Fig. 3.19	100	1.3E-04	0.030	100	p_{const}	383	327	298	304
82	5000	Fig. 3.19	10	1.3E-04	0.030	100	p_{const}	388	332	294	306
83	2000	Fig. 3.23	1000	6.7E-04	0.017	100	q_{const}	316	306	302	302
84	2000	Fig. 3.23	100	6.7E-04	0.017	100	q_{const}	318	306	303	305
85	2000	Fig. 3.23	10	6.7E-04	0.017	100	q_{const}	325	306	304	306

(0) Constant pressure or constant rate approach used in the Nobakht and Clarkson method (3).
(1) Regular time is used in the analysis.
(2) The modified Ibrahim and Wattenbarger method is used in the analysis.
(3) The Nobakht and Clarkson method is used in the analysis.
(4) The modified Behmanesh method is used in the analysis.

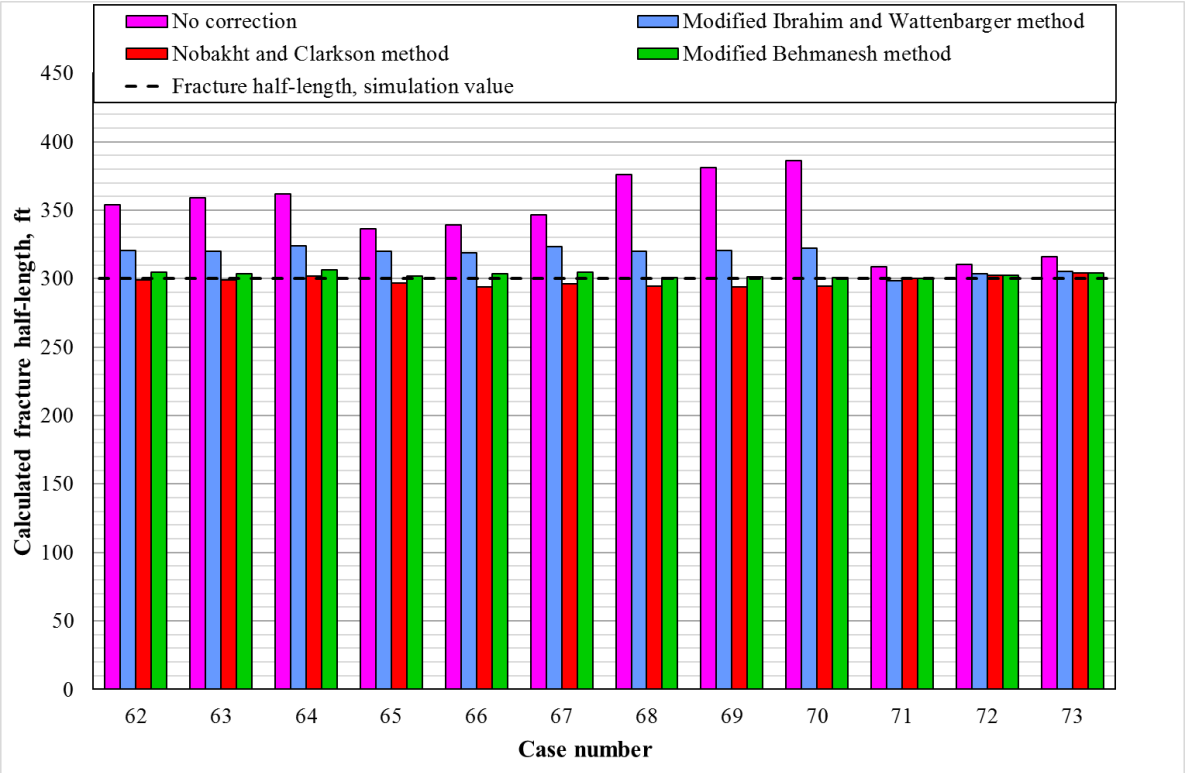

Fig. 3.15 - Calculated fracture half-lengths from the LFDP analysis on simulation cases 62 – 73.

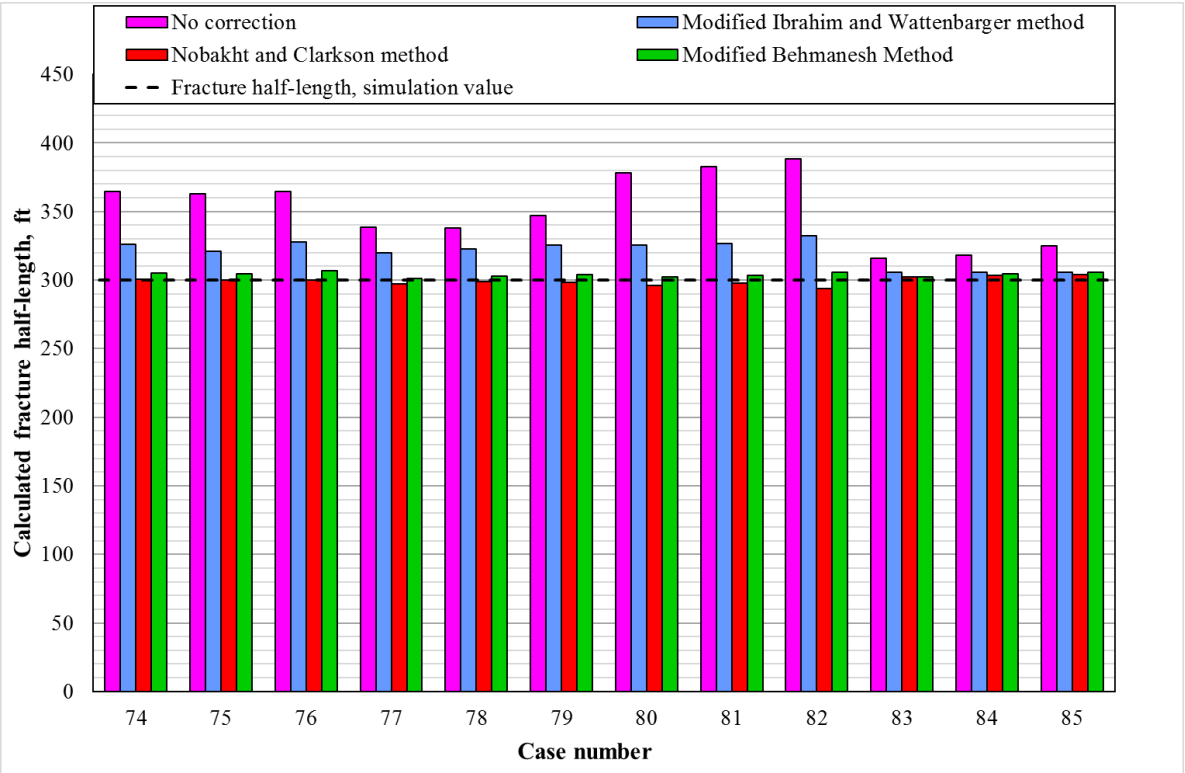

Fig. 3.16 - Calculated fracture half-lengths from the LFDP analysis on simulation cases 74 – 85.

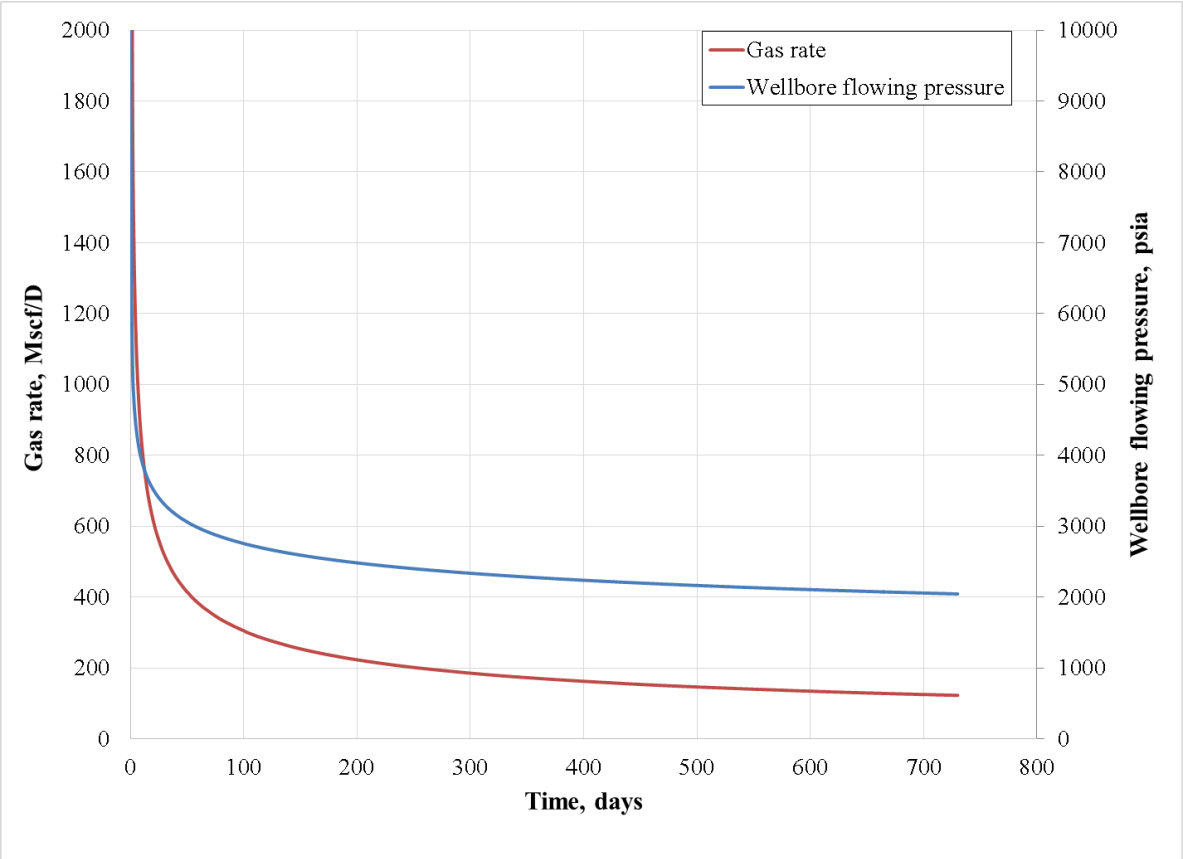

Fig. 3.17 - Wellbore pressure for cases 62 - 64 and 74 - 76 with the gas rates from case no. 63.

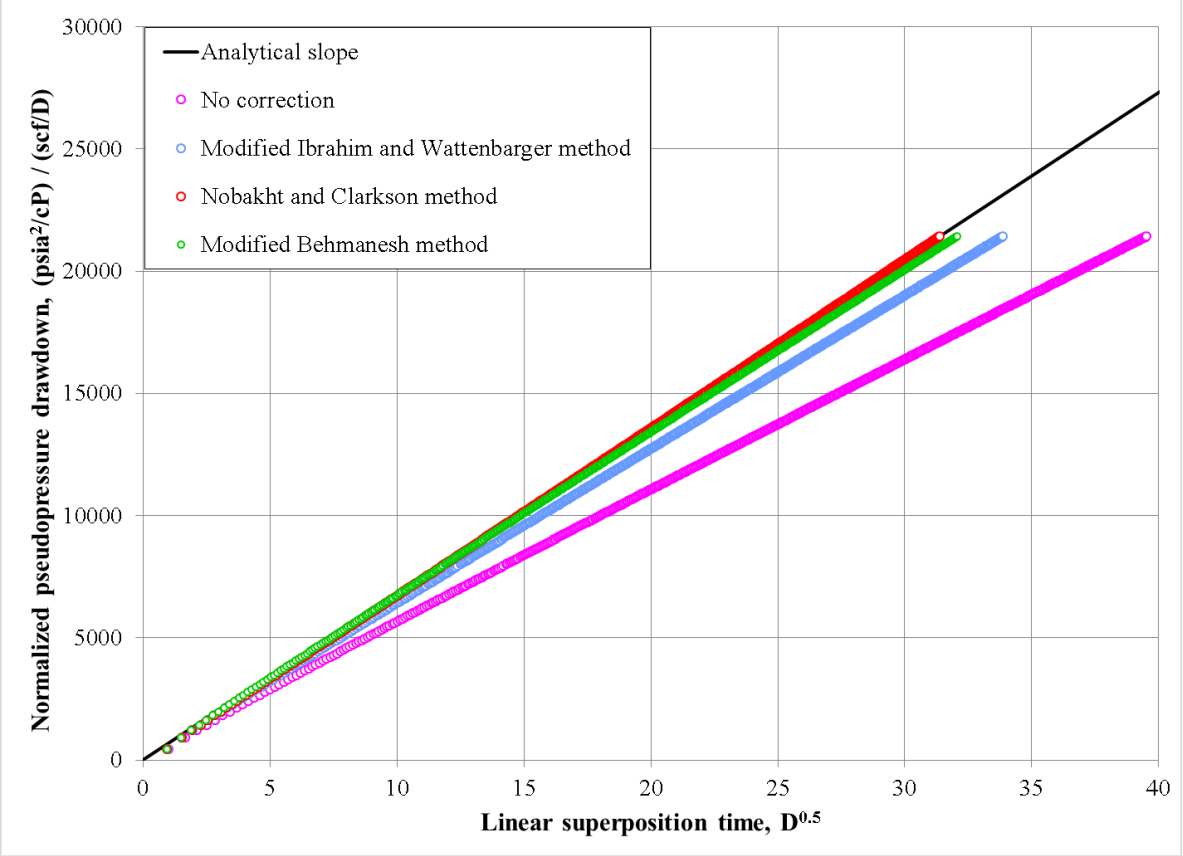

Fig. 3.18 - LFDP for simulation case no. 63.

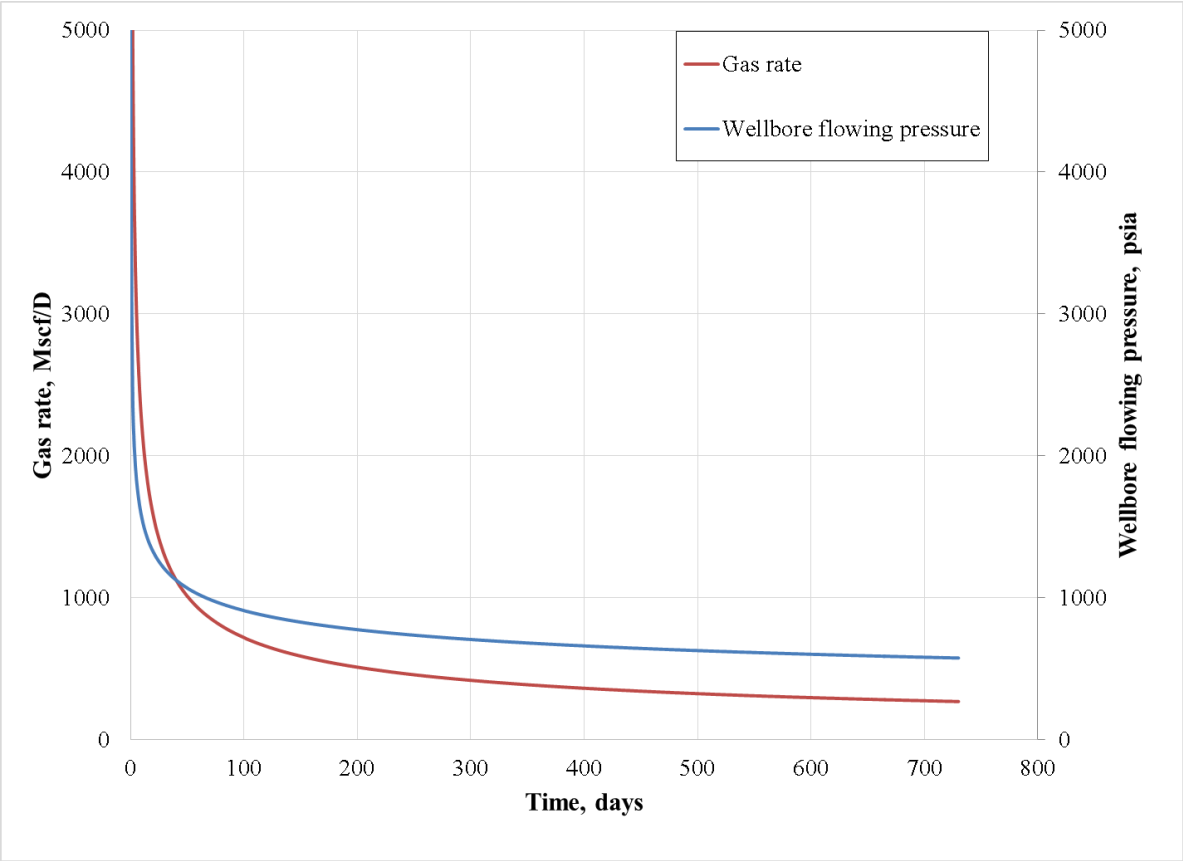

Fig. 3.19 - Wellbore pressure for cases 68 -70 and 80 - 82 with the gas rates from case no. 68.

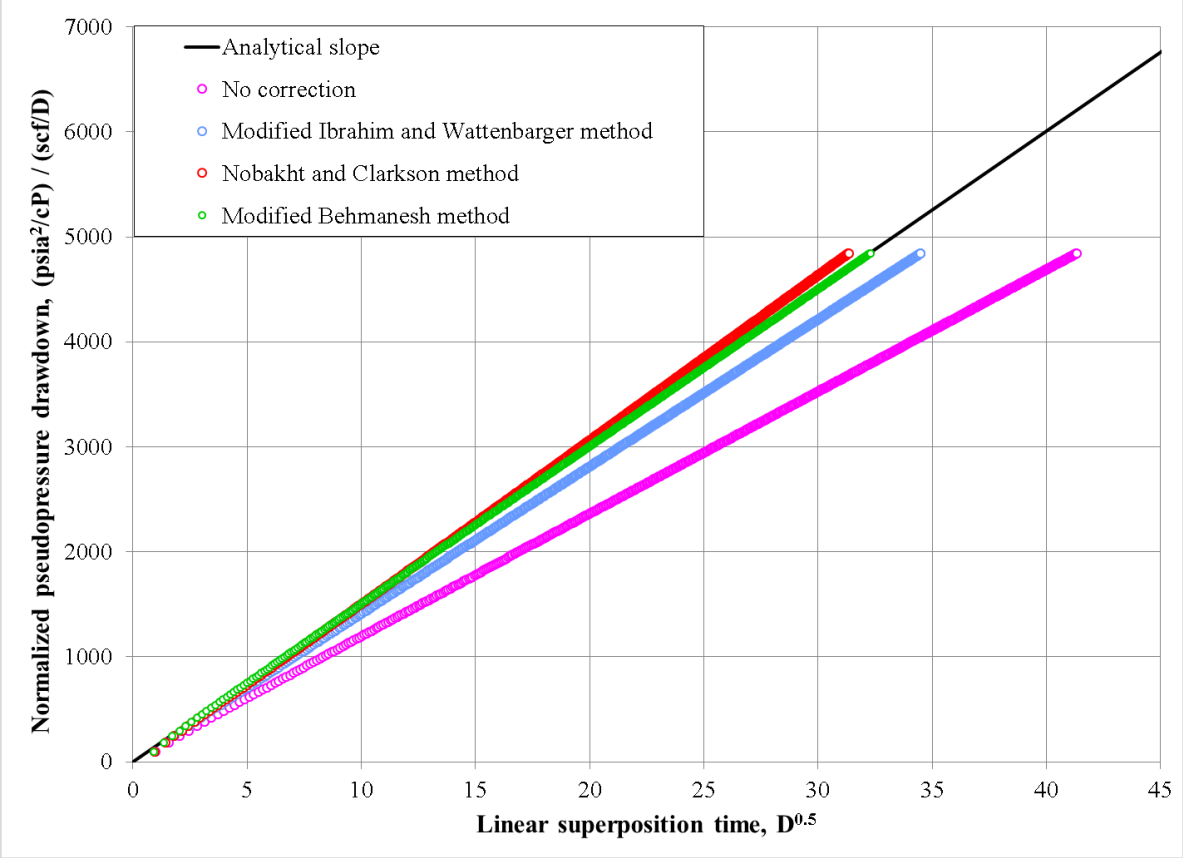

Fig. 3.20 - LFDP for simulation case no. 68.

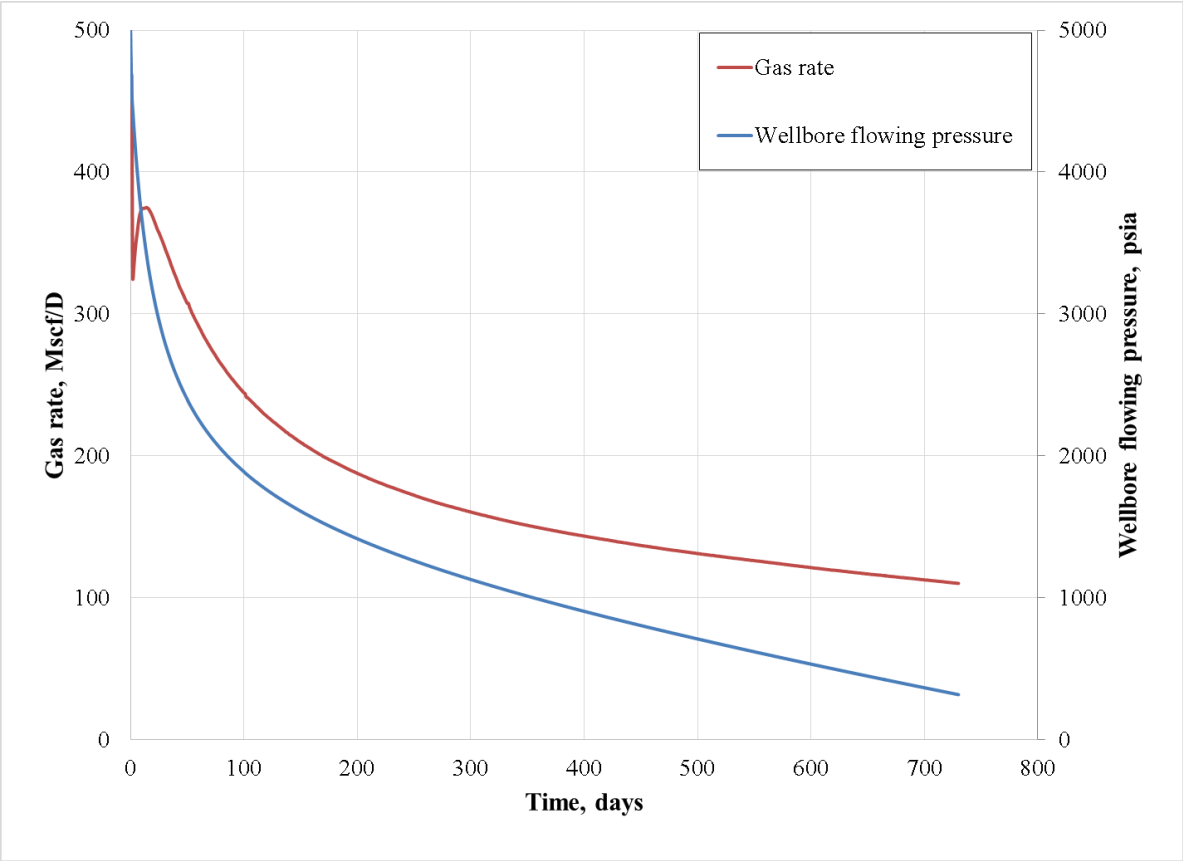

Fig. 3.21 - Wellbore pressure for cases 65 - 67 and 77 - 79 with the gas rates from case no. 78.

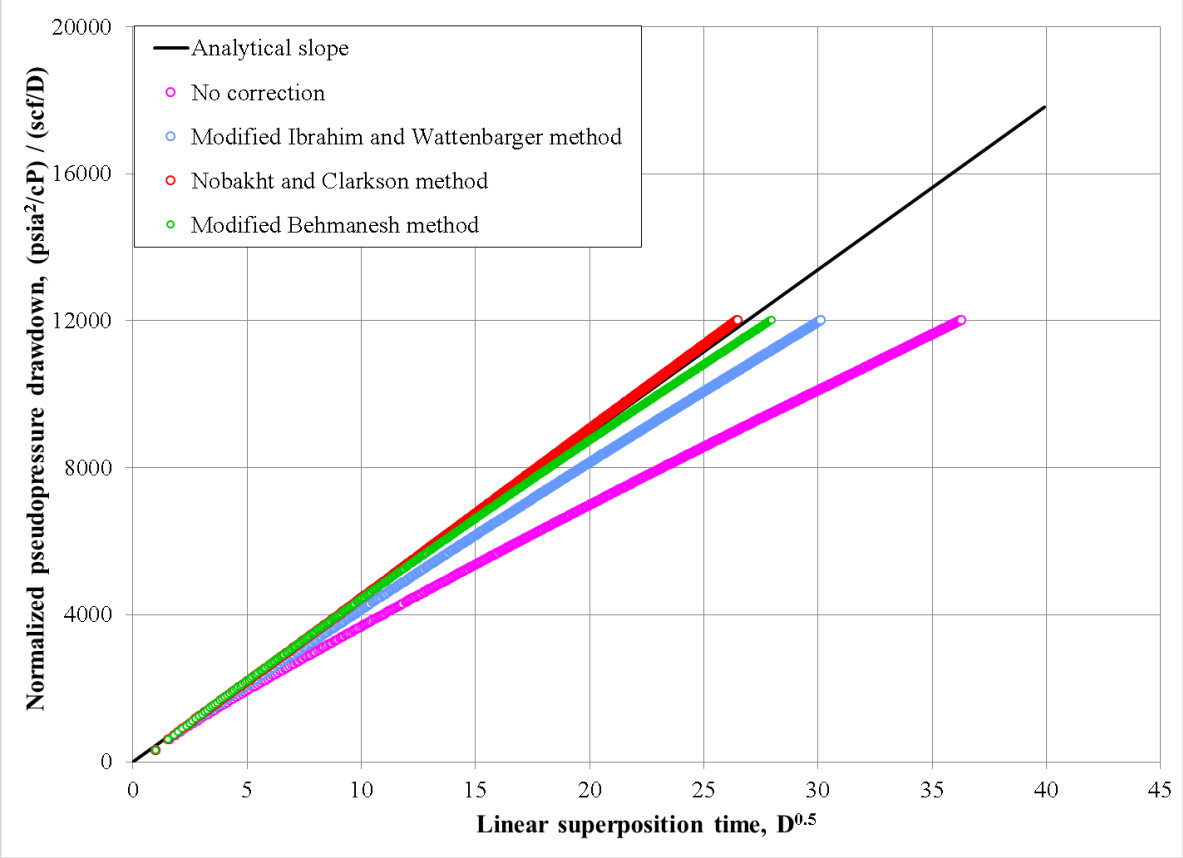

Fig. 3.22 - LFDP for simulation case no. 78.

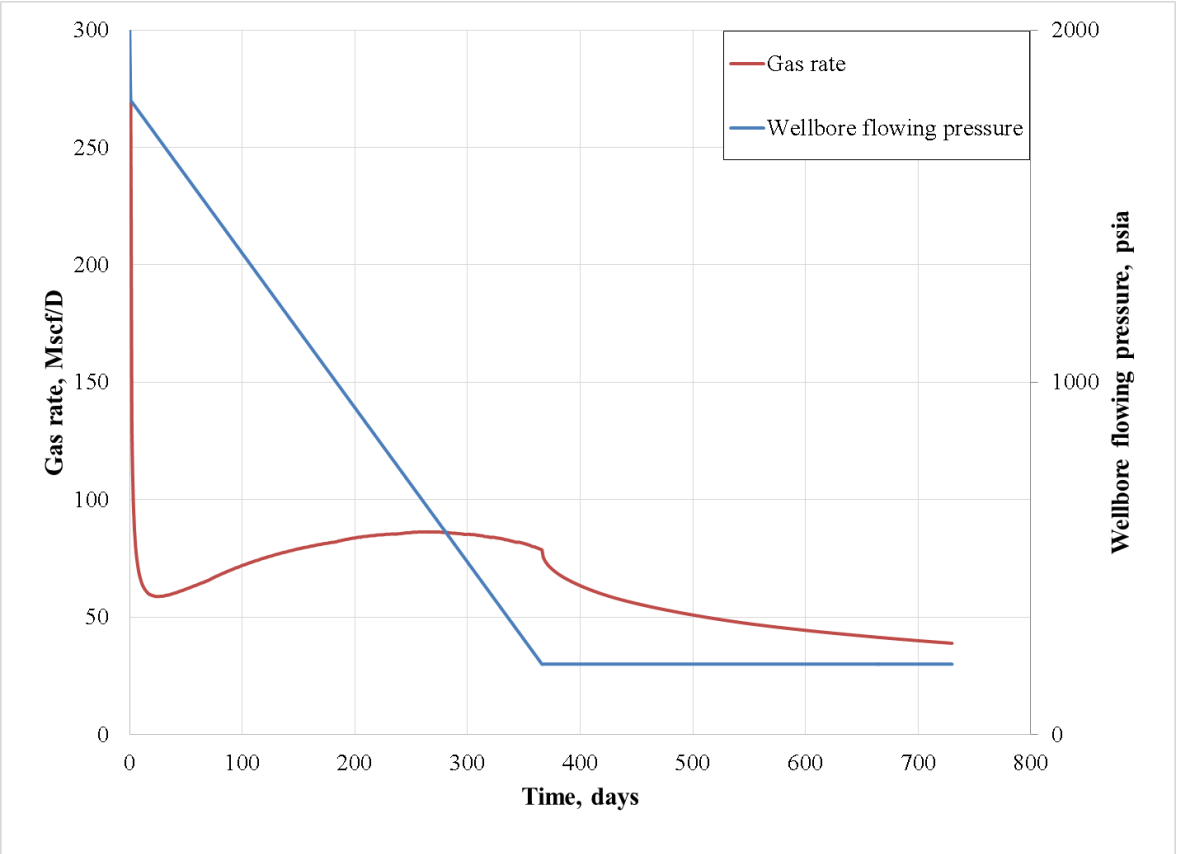

Fig. 3.23 - Wellbore pressure for cases 71 - 73 and 83 - 85 with the gas rates from case no. 84.

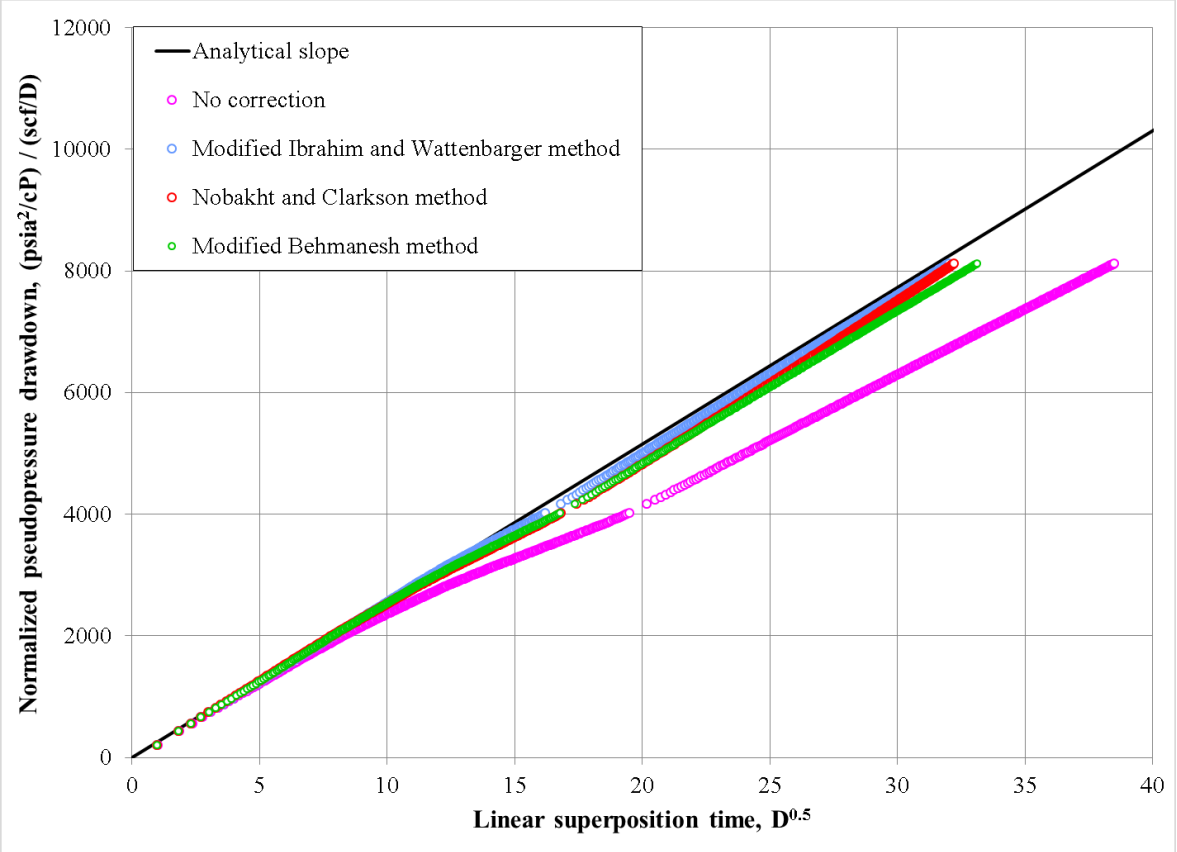

Fig. 3.24 - LFDP for simulation case no. 84.

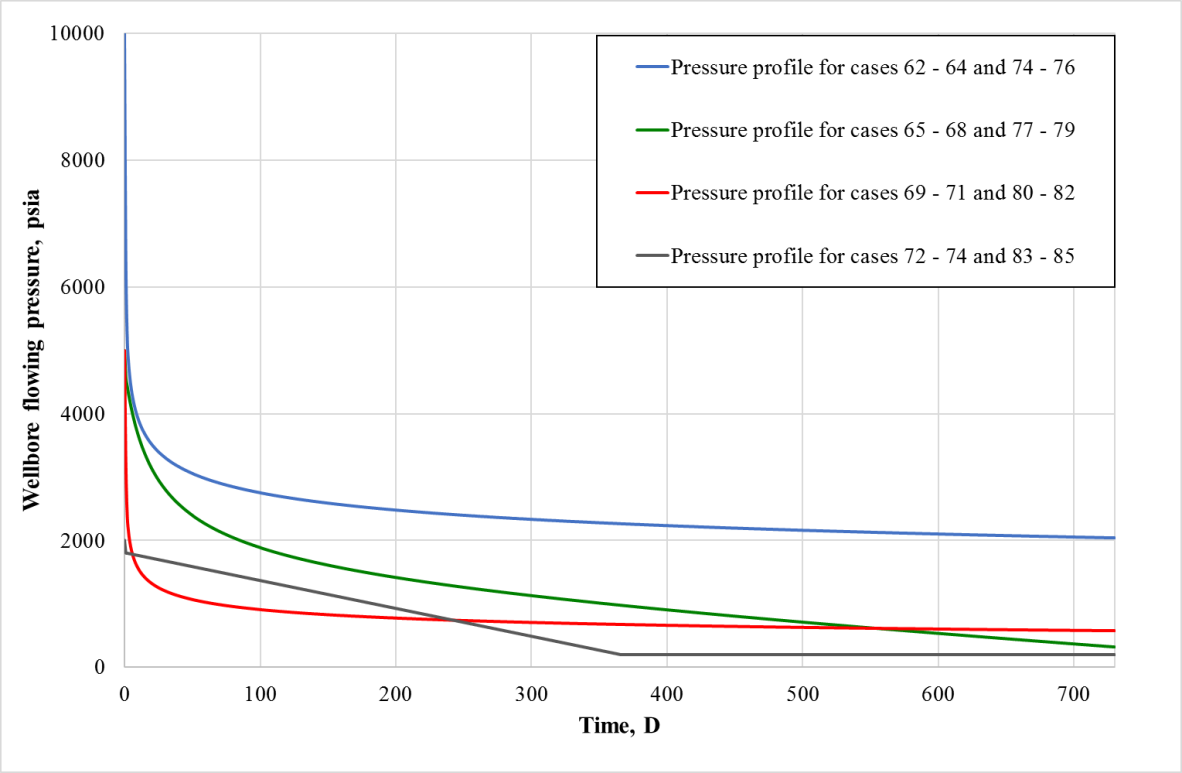

Fig. 3.25 - Flowing wellbore pressure profiles for simulation cases 62 - 85.

4 Discussion of Results

It is worth noting that the analysis method investigated in this work becomes a somewhat subjective exercise when the LFDP data does not fall on a straight line, and a straight line is to be fitted to the curving data. This non-linear trend in the LFDP was observed for some constant rate cases (e.g. Fig. 3.11) and some varying rate and flowing pressure cases (e.g. Fig. 3.22). It can be seen from these figures that the data corrected by the three investigated correction methods both plots closer to the expected analytical slope and shows more of a straight-line trend, making the straight-line curve fit more unique. The reported analysis results presented in Table 3 through Table 5 are based on manual straight-line fits to the data in the LFDP, where the early time data fit is prioritized when the plot shows curvature.

The following abbreviations will be used in this chapter: the Nobakht and Clarkson Method (NCM), the Ibrahim and Wattenbarger Method (IWM), and the Behmanesh Method (BM), referring to the previously described methods to correct for pressure dependent parameters in the dimensionless time expression. When no specific correction method is referenced to, data investigated with all four methods (uncorrected, the IWM, the NCM and the BM) is referred to.

4.1 Constant Flowing Pressure Production

As can be seen from Figs 3.1 through 3.3, the use of correction factors markedly improved the accuracy of the calculated fracture half-lengths. It is observed that the NCM and the BM yielded approximately equal fracture half-lengths in these constant pressure scenarios, with some instances of the NCM giving slightly better estimates. The IWM also improves the accuracy of the analysis, but the fracture half-length estimates are more imprecise than the ones provided by the NCM and the BM for most of the investigated cases.

By comparing Fig. 3.1 and Fig. 3.2, it is seen that the data corrected with the NCM and the BM are less affected than the uncorrected data and the data corrected by the IWM when adsorption was added to the analyzed data. The exception to this observation is seen in cases 16 – 18, where the IWM gave very good fracture half-length estimates. This is thought to be an artifact, as the IWM does not account for adsorbed gas. Except for the IWM data, the LFDP analysis was more adversely affected by desorption in cases 16 – 18 than in cases 10 – 15. This is believed to be instigated by the lower initial and flowing pressures in cases 16 - 18 causing more gas to be desorbed, as can be seen from the Langmuir curve, Fig. 2.5.

The pressure dependence of the data in the LFDP can be seen from Fig. 3.4 and Fig. 3.5, where a larger drawdown (Fig. 3.4) in an otherwise identical model (Fig. 3.5) causes a larger deviation between the analytical solution and the plotted data. In cases 24 and 25, where reservoir temperature is increased, an improvement in the fracture half-lengths calculated from the IWM is observed. This could be caused by the fact that the empirical Ibrahim and Wattenbarger (2005, 2006) correction factor was developed from data simulations performed with a reservoir temperature of 290 °F.

Increasing the formation compressibility to almost 50% of the gas compressibility, as is done in case 20, did not impact the NCM data or the BM data, which account for this effect in their correction factors, but significantly lowered the fracture half-lengths calculated without correction and from the data corrected with the IWM. This can possibly be explained by the total compressibility varying less for this scenario, as the constant formation compressibility term partly masks the varying gas compressibility.

The importance of including adsorption in the analysis when it is present in the reservoir is displayed in Fig. 3.7, where failing to account for adsorption causes large deviations between the analytical slope and the LFDP data.

4.2 Constant Rate Production

In general, the calculated fracture half-lengths for the constant rate production scenarios were closer to the simulation values than what was found in the constant pressure analysis. A likely explanation for this is that at early times, the drawdown required to maintain a constant rate is not as high as in the constant pressure cases investigated. Because of this property, the early time data from which the slope value is extracted will only be slightly affected by the pressure dependent gas and reservoir properties, giving better fracture half-length estimates. This effect is also believed to be the reason cases 40 – 45 were almost unaffected by the presence of adsorption, as only small amounts of gas was desorbed at early times. Cases 46 – 48 (p_i = 2000 psia) are slightly more affected by adsorption, as explained in the previous section. It is seen from Fig. 3.11 that all the late time data in the LFDP curves downwards, and that the uncorrected data shows more curvature and departs from the analytical slope at early times. The rate dependence of the LFDP analysis is seen from Fig. 3.12, which shows the same reservoir model as presented in Fig. 3.11, produced at a smaller flow rate, where the data corrected with the NCM and the modified BM falls on a straight line close to the analytical slope, while the modified IWM and the uncorrected data still show some (less severe) curvature.

When increasing reservoir temperature, the same effect as was seen in the constant pressure data was seen in simulation cases 54 and 55, where the modified IWM yielded better fracture half-length estimates at higher temperatures. Increasing the formation compressibility, as is done in case 53, showed (to a smaller degree) the same results as were observed in the constant pressure investigation. Ignoring the presence of adsorption in the LFDP analysis was shown to severely impact the investigation results also for constant rate production, as is seen in Fig. 3.13.

4.3 Variable Rate and Flowing Pressure Production

For the variable rate and flowing pressure scenarios investigated in this work, the NCM and the modified BM yielded similar results, with the fracture half-length estimated from these methods generally closer to the simulation value than what was observed in the modified IWM and the uncorrected data. It can be seen in Fig. 3.18 and Fig. 3.22 that the data corrected with the modified BM showed some of the same tendencies as was seen in the constant rate data, where the late time data curves downwards, while still being able to achieve a good straight-line fit to the straight early time data trend. In Fig. 3.20 it is seen that the modified BM traces the analytical slope, while the NCM "overcorrects" the data. As observed in the constant rate and constant flowing pressure analysis, desorption did not have a large effect on the data corrected with the NCM and the modified BM, while the modified IWM and the uncorrected data were more adversely affected. The effect of desorption was more prominent in the low initial pressure cases, 83 – 85, as was observed in the constant rate and constant pressure investigations.

5 Conclusions

The straight-line method studied in this work showed good ability to estimate the fracture half-length used to generate simulated gas production data for a series of constant rate, constant pressure and varying rate and pressure scenarios, when the data was corrected for the pressure dependent parameters found in the diffusivity term, $k/(\phi\mu c_t)$. Of the three correction methods investigated in this work, the best results were achieved from the methodology proposed by Nobakht and Clarkson (2011a, 2011b, 2011c) and Nobakht et al. (2011), and the method proposed by Behmanesh (2016), modified in this work to be applicable to varying pressure conditions. The advantage of the modified Behmanesh (2016) method is that it is easily applicable and is not an iterative procedure. The third investigated method, proposed by Ibrahim and Wattenbarger (2005, 2006) and modified by Nystad (2015) to be used for varying pressure data, was found to improve the results from the analysis method when compared to uncorrected data, but these results were less accurate than the results from the two aforementioned correction methods.

6 References

Agarwal, R. G. (1979, January 1). “Real Gas Pseudo-Time” - A New Function for Pressure Buildup Analysis of MHF Gas Wells. Society of Petroleum Engineers. doi:10.2118/8279-MS

Al-Hussainy, R., Ramey, H. J., & Crawford, P. B. (1966, May 1). The Flow of Real Gases Through Porous Media. Society of Petroleum Engineers. doi:10.2118/1243-A-PA

Anderson, D. M., & Mattar, L. (2005, January 1). An Improved Pseudo-Time for Gas ReservoirsWith Significant Transient Flow. Petroleum Society of Canada. doi:10.2118/2005-114

Arevalo-Villagran, J. A., Cinco-Ley, H., Wattenbarger, R. A., Garcia-Hernandez, F., & Samaniego-Verduzco, F. (2003, January 1). Transient Analysis of Tight Gas Well Performance - More Case Histories. Society of Petroleum Engineers. doi:10.2118/84476-MS

Bello, R. O. (2009). Rate transient analysis in shale gas reservoirs with transient linear behavior. PhD Dissertation, Texas A&M University.

Behmanesh, H. (2016, January 27). Rate-Transient Analysis of Tight Gas Condensate and Black Oil Wells Exhibiting Two-Phase Flow. PhD Dissertation, University of Calgary. http://hdl.handle.net/11023/2782

Behmanesh, H., Clarkson, C. R., Tabatabaie, S. H., & Heidari Sureshjani, M. (2015, December 1). Impact of Distance-of-Investigation Calculations on Rate-Transient Analysis of Unconventional Gas and Light-Oil Reservoirs: New Formulations for Linear Flow. Society of Petroleum Engineers. doi:10.2118/178928-PA

Behmanesh, H., Tabatabaie, S. H., Heidari Sureshjani, M., & Clarkson, C. R. (2014, April 1). Modification of the Transient Linear Flow Distance of Investigation Calculation for Use in Hydraulic Fracture Property Determination. Society of Petroleum Engineers. doi:10.2118/168981-MS

Bumb, A. C., & McKee, C. R. (1988, March 1). Gas-Well Testing in the Presence of Desorption for Coalbed Methane and Devonian Shale. Society of Petroleum Engineers. doi:10.2118/15227-PA

Clarkson, C.R. (2013). Production data analysis of unconventional gas: Review of theory and best practices. International Joural of Coal Geology 109-110:191-146. DOI: 10.1016/j.coal.2013.01.002

Clarkson, C. R., & Beierle, J. (2010, January 1). Integration of Microseismic and Other Post-Fracture Surveillance with Production Analysis: A Tight Gas Study. Society of Petroleum Engineers. doi:10.2118/131786-MS

Clarkson, C. R., & Pedersen, P. K. (2010, January 1). Tight Oil Production Analysis: Adaptation of Existing Rate-Transient Analysis Techniques. Society of Petroleum Engineers. doi:10.2118/137352-MS.

Daungkaew, S., Hollaender, F., & Gringarten, A. C. (2000, January 1). Frequently Asked Questions in Well Test Analysis. Society of Petroleum Engineers. doi:10.2118/63077-MS

Fetkovich, M. J., & Vienot, M. E. (1984, December 1). Rate Normalization of Buildup Pressure by Using Afterflow Data. Society of Petroleum Engineers. doi:10.2118/12179-PA

Fraim, M. L. & Wattenbarger, R. A. (1987, December 1). Gas Reservoir Decline-Curve Analysis Using Type Curves with Real Gas Pseudopressure and Normalized Time. Society of Petroleum Engineers. doi:10.2118/14238-PA

Gringarten, A. C., Ramey, H. J., & Raghavan, R. (1974, August 1). Unsteady-State Pressure Distributions Created by a Well With a Single Infinite-Conductivity Vertical Fracture. Society of Petroleum Engineers. doi:10.2118/4051-PA

Ibrahim, M., & Wattenbarger, R. A. (2005, January 1). Analysis of Rate Dependence in Transient Linear Flow in Tight Gas Wells. Petroleum Society of Canada. doi:10.2118/2005-057

Ibrahim, M. H., & Wattenbarger, R. A. (2006, January 1). Analysis of Rate Dependence in Transient Linear Flow in Tight Gas Wells. Society of Petroleum Engineers. doi:10.2118/100836-MS

Langmuir, I. 1918. The Adsorption of Gases on Plane Surfaces of Glass, Mica and Platinum. Journal of American Chemical Society 40. doi:10.1021/ja02242a004

Leahy-Dios, A., Das, M., Agarwal, A., & Kaminsky, R. D. (2011, January 1). Modeling of Transport Phenomena and Multicomponent Sorption for Shale Gas and Coalbed Methane in an Unstructured Grid Simulator. Society of Petroleum Engineers. doi:10.2118/147352-MS

Kanfar, M., Alkouh, A. B., & Wattenbarger, R. A. (2013, August 20). Modeling Guidelines for Analyzing and Forecasting Shale Well Performance. Society of Petroleum Engineers. doi:10.2118/165698-MS

King, G. R. (1993, February 1). Material-Balance Techniques for Coal-Seam and Devonian Shale Gas Reservoirs with Limited Water Influx. Society of Petroleum Engineers. doi:10.2118/20730-PA

Kuchuk, F. J. (2009, January 1). Radius of Investigation for Reserve Estimation From Pressure Transient Well Tests. Society of Petroleum Engineers. doi:10.2118/120515-MS

Moghadam, S., Jeje, O., & Mattar, L. (2011, January 1). Advanced Gas Material Balance in Simplified Format. Society of Petroleum Engineers. doi:10.2118/139428-PA

Muskat, M. 1937. The Flow of Homogeneous Fluids Through Porous Media. New York, McGraw-Hill Book Co. Ch. 3.5, p. 135.

Nobakht, M., & Clarkson, C. R. (2011a, January 1). A New Analytical Method for Analyzing Production Data from Shale Gas Reservoirs Exhibiting Linear Flow: Constant Pressure Production. Society of Petroleum Engineers. doi:10.2118/143989-MS

Nobakht, M., & Clarkson, C. R. (2011b, January 1). A New Analytical Method for Analyzing Production Data from Shale Gas Reservoirs Exhibiting Linear Flow: Constant Rate Production. Society of Petroleum Engineers. doi:10.2118/143990-MS

Nobakht, M., & Clarkson, C. R. (2011c, January 1). Analysis of Production Data in Shale Gas Reservoirs: Rigorous Corrections for Fluid and Flow Properties. Society of Petroleum Engineers. doi:10.2118/149404-MS

Nobakht, M., Clarkson, C. R., & Kaviani, D. (2011, January 1). New and Improved Methods for Performing Rate-Transient Analysis of Shale Gas Reservoirs. Society of Petroleum Engineers. doi:10.2118/147869-MS

Nystad, M. (2015). Analysis of Linear Gas Flow in Unconventional Reservoirs, NTNU.

Odeh, A. S., & Jones, L. G. (1965, August 1). Pressure Drawdown Analysis, Variable-Rate Case. Society of Petroleum Engineers. doi:10.2118/1084-PA

Shahamat, M. S., Mattar, L., & Aguilera, R. (2014, February 25). A Physics-Based Method for Production Data Analysis of Tight and Shale Petroleum Reservoirs Using Succession of Pseudo-Steady States. Society of Petroleum Engineers. doi:10.2118/167686-MS

Sing, K. S. W., Everett, D. H., Haul, R. A. W., Moscou, L., Pierotti, R. A., Rouquerol, J. and Siemieniewska, T. 1985. Reporting Physisorption Data for Gas/Solid Systems with Special Reference to the Determination of Surface Area and Porosity (Recommendations 1984). Pure and Applied Chemistry 57 (4): pp. 603-619. doi:10.1351/pac198557040603

Wattenbarger, R. A., El-Banbi, A. H., Villegas, M. E., & Maggard, J. B. (1998, January 1). Production Analysis of Linear Flow Into Fractured Tight Gas Wells. Society of Petroleum Engineers. doi:10.2118/39931-MS

Whitson, C. H., Coll, C., Dahouk, M. M., & Juell, A. O. (2016, May 30). Shale Reserve Forecasting - Model Consistency and Uncertainty. Society of Petroleum Engineers. doi:10.2118/180140-MS

7 Nomenclature and Abbreviations

Abbreviations

BM - Behmanesh Method
DOI - Distance of Investigation.
LFDP - Linear Flow Diagnostic Plot, see Eq. 2.14.
LFP - Linear Flow Parameter, product of square root of time and fracture half-length.
IWM - Ibrahim and Wattenbarger Method
NCM - Nobakht and Clarkson Method
PSS - Pseudo Steady State.

Nomenclature

A - Area, ft^2.
b - Slope intercept on linear flow diagnostic plot, see Eq. 2.17.
B_g - Gas formation volume factor, ft^3/scf.
B_g^* - Modified gas formation volume factor, ft^3/scf, see Eq. 2.38.
c_d - Adsorption compressibility, psi^{-1}, see Eq. 2.29.
c_f - Formation compressibility, psi^{-1}.
c_g - Gas compressibility, psi^{-1}.
c_t - Total system compressibility, psi^{-1}.
D_D - Dimensionless drawdown, see Eq. 2.31.
D_D^* - Modified dimensionless drawdown, see Eq. 2.33.
f_{CP} - Dimensionless correction factor, see Eq. 2.43.
$f_{CP,IW}$ - Empirical correction factor, dimensionless, see Eq. 2.30.
f_{CP}^* - Modified empirical correction factor, dimensionless, see Eq. 2.32.
f_{CP}^{**} - Dimensionless correction factor, see Eq. 2.49.
F_c - Fracture conductivity, md-ft.
F_{CD} - Dimensionless fracture conductivity.
G - Contacted gas in place, scf, see section 2.5.2.
G_p - Gas produced, scf.
h - Height, ft.
k - Permeability, md.
k_f - Fracture permeability, md.
m_{CR} - Slope of linear flow diagnostic plot, see Eq. 2.15.
m_{CP} - Slope of square root of time plot, see Eq. 2.20.
p_D - Dimensionless pressure.
p_{Dc} - Dimensionless pressure constant, see Eq. 2.7.
p - Pressure, psia.
p_i - Initial reservoir pressure, psia.
$p_p(p)$ - Pseudopressure evaluated at pressure p, $psia^2/cP$.
$p_p(p_i)$ - Pseudopressure evaluated at the initial pressure, $psia^2/cP$.
$p_p(p_{wf})$ - Pseudopressure evaluated at the flowing wellbore pressure, $psia^2/cP$.
$p_p(\bar{p})$ - Pseudopressure evaluated at the average pressure, $psia^2/cP$.
p_{wf} - Flowing wellbore pressure, psia.
p_L - Langmuir pressure, psia, see Eq. 2.27.
p_0 - Reference pressure, psia.
$\bar{p}$ - Average pressure, evaluated in region of influence, psia.
q - Fluid flow rate, units depend on fluid type (e.g. scf/D, STB/D).

q_g - Gas flow rate, scf/D.
q_i - Initial gas flow rate, scf/D.
q_D - Dimensionless rate.
s - Dimensionless steady state skin factor.
t - Time, Days.
t_a - Corrected pseudotime, Day, see Eq. 2.33.
$t_{a,CP}$ - Corrected pseudotime for constant pressure production, Day, see Eq. 2.23.
t_D - Dimensionless time.
t_{Dxf} - Dimensionless time for a fractured well, see Eq. 2.6.
t_{Dxfc} - Dimensionless time constant for a fractured well, Day^{-1}, see Eq. 2.6.
t_{LS} - Linear superposition time, $Day^{0.5}$, see Eq. 2.13.
$t_{a,LS}$ - Linear superposition pseudotime, $Day^{0.5}$, see Eq. 2.26.
t^* - Pseudotime evaluated at the wellbore, Day, see Eq. 2.22.
t_{LS}^* - Linear superposition time with the modified Ibrahim and Wattenbarger correction, $Day^{0.5}$, see Eq. 2.34.
t_{LS}^{**} - Linear superposition time with the modified Behmanesh correction, $Day^{0.5}$, see Eq. 2.50
T - Temperature, °R.
V_a - Adsorbed volume, scf/ton, see Eq. 2.27.
V_L - Langmuir volume, scf/ton, see Eq. 2.27.
w_f - Fracture width, ft.
x_e - Distance from wellbore to end of drainage area parallel to fracture, ft.
x_f - Fracture half-length, ft.
y - Distance from fracture, ft.
y_e - Distance between fracture and no-flow boundary, ft.
y_{inv} - Investigated distance, measured from fracture, ft, see Eq. 2.21.
y_D - Dimensionless distance.
Z - Real gas deviation factor, dimensionless.
Z^* - Modified real gas deviation factor, dimensionless, see Eq. 2.36.
$\bar{Z}^*$ - Modified real gas deviation factor evaluated at the average pressure.
Z^{**} - Modified real gas deviation factor, dim. less, see Moghadam et al. (2011).

Greek symbols

α - Distance of investigation constant, dimensionless, see Eq. 2.21.
δ - Partial derivative operator.
Δp_p - Pseudopressure at wellbore subtracted from initial pseudopressure, $psia^2/cP$.
μ - Viscosity, cP.
ρ_B - Formation density, g/cm^3.
ϕ - Porosity, fraction.

Subscripts

CP - Constant pressure.
CR - Constant rate.
i - Initial conditions.
j - Index of summation.
LS - Linear superposition.
n - Upper bound of summation.
sc - Standard conditions.